# Single and mixed gas permeability studies on mixed matrix membranes composed of MIL-101(Cr) or MIL-177(Ti) and highly permeable Polymers of Intrinsic Microporosity.

*Elisa Esposito[1*], Mariolino Carta[2*], Alessio Fuoco[1], Marcello Monteleone[1], Bibiana Comesaña-Gándara[3], Effrosyni Gkaniatsou[4], Clémence Sicard[4], Sujing Wang[5], Christian Serre[5], Neil B. McKeown[3], Johannes C. Jansen[1]*

[1]Institute on Membrane Technology, CNR-ITM, Via P. Bucci 17/C, 87036 Rende (CS), Italy. E-mail: e.esposito@itm.cnr.it

[2]Department of Chemistry, Faculty of Science and Engineering, Swansea University, Swansea, SA2 8PP, UK

[3]EastChem, School of Chemistry, University of Edinburgh, Edinburgh EH9 3FJ, UK

[4]Institut Lavoisier de Versailles, UVSQ, CNRS, Université Paris-Saclay, 78035 Versailles, France

[5]Institut des Matériaux Poreux de Paris, UMR 8004 CNRS Ecole Normale Supérieure, Ecole Supérieure de Physique et de Chimie Industrielles de Paris, PSL research university, 75005 Paris, France.

**Abstract**

The gas transport properties of mixed matrix membranes (MMMs), prepared by dispersing nanoparticles of MOFs MIL-101(Cr) or MIL-177(Ti) into highly permeable Polymers of Intrinsic Microporosity PIM-EA-TB or PIM-TMN-Trip, were investigated. The homogeneity of the dispersion was confirmed by means of Scanning Electron Microscopy (SEM) and Energy-dispersive X-ray (EDX) mapping analysis. Single gas time-lag measurements provided the permeability and ideal selectivity of different gas pairs, both after treatment of the MMMs with methanol and after natural aging over an extended period (up to 2000 days). This data demonstrated that the gas size-sieving pores of MIL-101(Cr) and MIL-177(Ti) and their good dispersion into the PIM matrix results in MMMs with enhanced gas separation performance, as compared to films composed solely of the polymer. The comparison of actual permeability with Maxwell model for PIM-EA-TB with both MOFs confirmed the good dispersion and the absence of anomalies, whereas the inconsistency of permeability with prediction data for PIM-TMN-Trip suggests that the MOFs improved the polymer properties, stiffening or occupying

the polymer free volume. In particular, the incorporation of MIL-101(Cr) into PIM-EA-TB significantly enhances the $H_2$ permeability from ~ 6000 to 13000 Barrer, with a concurrent increase of the $H_2/N_2$ selectivity from 14 to 21. MIL-177(Ti) also enhances the $H_2/N_2$ selectivity to 20 due to a slight reduction of the $N_2$ permeability. The addition of MIL-101(Cr) and MIL-177(Ti) into the ultra-permeable PIM-TMN-Trip showed more modest increases in $H_2$ permeability and $H_2/N_2$ selectivity from 4.6 to ~ 10. Hence the data for some of the MMMs surpass the 2008, and even approach the 2015/2019 Robeson's upper bounds, particularly for gas pairs including $H_2$.

**Keywords**: Mixed matrix membranes, PIMs, MOFs, MIL-101(Cr), MIL-177(Ti), gas separation, Maxwell model

## 1 Introduction

Membranes derived from Polymers of Intrinsic Microporosity (PIMs) have demonstrated promise for gas separations [1–5]. This is mainly attributable to their high permeability, often paired with good selectivities for several commercially important gas pairs. Their remarkable gas transport performance of PIMs can be attributed to their unique structural design inspired by the pioneering theoretical insight of Freeman [6]. He proposed that high permeability ($PA$) and good selectivity ($\alpha_{(A/B)}$) in polymeric membranes requires a combination of high free volume and stiff polymer chains. PIM-1, the archetypal example of this class of materials, exemplifies this concept as it features a fused-ring structure that imparts high stiffness to the backbone, and a spiro-centre that provides the site of contortion, necessary to induce microporosity and free volume [7,8]. This combination allowed the gas permeability data of PIM-1 to define the 2008 Robeson's upper bounds [9]. Since then, many chemical and structural modifications of PIM-1, aimed to improve their gas performance, have been proposed [10]. For instance, chemical modification of the nitrile-group led to obtain amine- [11,12], thioamide- [13], amidoxime- [14], and tetrazole-functionalized PIM-1 (TZPIM) [15], all of which showed an improved affinity for $CO_2$ and, as consequence, an enhanced selectivity for $CO_2$ based gas pairs. The incorporation of Tröger's Base (TB) units into PIMs initiated the synthesis of a new family of, so-called TB-PIMs, such as PIM-EA-TB that was used in this study ($PCO_2$ ~6000 Barrer, $\alpha CO_2/N_2$=13) [3,16]. The introduction of rigid and extended "spacer" groups into novel TB-PIMs, provided additional inter-chain separation that contributed to the synthesis of even more permeable PIMs, such as PIM-BTrip-TB and PIM-TMN-Trip-TB [17–19]. A similar increase of the performance of benzodioxin-linked PIMs was achieved by

incorporating triptycene units, especially those linked to "spacer units". For example, PIM-TMN-Trip [17] exhibits comparable permeability to the much studied ultrapermeable poly(trimethylsilylpropyne) but with significantly higher selectivity, which was attributed to its pronounced size-sieving effect originating from its highly rigid chain structure [20]. More recently, the replacement of the TMN with a variety of functional groups led to the development of a new series of benzotriptycene-PIMs with tailored permeability and selectivity. These advancements led to the proposed revisions to the Robeson upper bounds for $CO_2$ based gas pairs [21] which has set a high benchmark for recently developed PIMs [22]. Despite their exciting initial performance, all PIMs are susceptible to the phenomenon of aging, which refers to a process that occurs in glassy polymers when stored at temperatures lower than their glass transitions [28]. Typically, polymer chains are initially "frozen" in a non-equilibrium thermodynamic state, which creates a high free volume in the material. However, over time (often just a few weeks), these chains relax and approach equilibrium, altering their spatial arrangement and leading to the loss of part of the free volume, with a consequent decrease in permeability often compensated with an increased selectivity for selected gas pairs [29].

An effective technique for boosting the performance of PIMs for gas separation involves the incorporation of insoluble nanoparticles (known as fillers) into a soluble PIM (the matrix), which leads to the formation of mixed matrix membranes (MMMs). Their combination aims to synergistically enhance both permeability and selectivity, along with mitigating aging [23,24]. The solution-diffusion model, which typically describes the gas transport in PIMs membranes, suggests that permeability of a gas through a dense polymer is the result of contribution from both gas diffusion and gas solubility ($P = D * S$). Hence, the introduction of porous fillers such as MOFs may increase the overall performance, simultaneously enhancing both parameters[25]. In fact, MOFs with well-defined pores can improve the diffusion of smaller gases, thus influencing the overall selectivity via an improved diffusivity selectivity ($D_A/D_B$). In addition, MOFs can bear substituents which are aimed to enhance the affinity for specific gases. In this case the selectivity would be primarily affected by an improved solubility selectivity ($S_A/S_B$) [23,26,27]. The presence of MOFs, along with the improvement of initial permeability and selectivity, may also influence the local polymer dynamics, mitigating the gradual loss of free volume and, thus reducing aging [24,30,31]. Several research groups have explored this approach by dispersing a variety of crystalline compounds in PIM-based membranes, such as porous organic frameworks (POFs) [24], zeolitic imidazolate frameworks (ZIF) [32–35], and metal organic frameworks (MOFs) [36–41]. For example, the addition of

ZIF-8 into PIM-1 pushed its performance above the 2008 upper bound for several gas pairs, which was predominantly attributed an improvement of the diffusion selectivity [33]. Hao et al. studied MMMs based on the combination of PIM-1 and ZIF-71, finding that the dispersion of the filler of up to 30 wt% improves the $CO_2$ permeability from ~ 3000 to 8000 Barrer, without apparent loss of selectivity. In the attempt to mitigate the aging process, Lau at al., incorporated the porous aromatic framework PAF-1 into PIM-1 resulting in a selectivity increase with aging, without apparent loss of permeability [24]. Khdhayyer et al. and Ghalei at al., improved on the performance of PIM-1 towards $CO_2$ by incorporating zirconium-based MOF UiO-66 [40,42]. Yampolskii et al., dispersed MIL-101 into PIM-1, leading to the increase the permeability of most gases, which they attributed to the enhancement of the diffusion due to the insertion of the MOF [36], which is in agreement with work of Khdhayyer et al. [37]. Recently, Chen et al., incorporating KAUST-7 into PIM-1 produced MMMs with long-term stablility for $CO_2/CH_4$ separation [23].

To the best of our knowledge, here we report the performance of the first MMMs prepared from two important MOFs, namely MIL-101(Cr) and MIL-177(Ti), with the highly permeable PIM-EA-TB and PIM-TMN-Trip as polymer matrices. These two fillers were selected based on (i) the ability to be synthetized as homogenous nanoparticles, which is crucial to ensure their homogenous dispersion in MMMs; (ii) their excellent chemical stability and (iii) their large pore sizes, each with unique pore morphologies. In fact, MIL-101(Cr) shows 3D mesoporous cages (2.9 nm and 3.4 nm of diameter), accessible by windows of 1.6 and 1.2 nm [43], whereas MIL-177(Ti) possesses 1D hexagonal channels of ca 1.1 nm of diameter, along with narrow (ca. 0.3 nm) 1D channel (Fig. 1A-B) [44]. MIL-101(Cr) is one of the most studied MOFs, particularly for applications in gas separation [45]. The gas transport properties of MMMs were tested via ***single gas*** permeation measurements in different membrane conditions, such as freshly ***MeOH treated*** (which is known to reset the history of the film casting), after ***thermal treatment*** (which is known to accelerate the aging), after long ***natural aging*** (in some cases, after several years) and under real ***mixed gas conditions***. All these experiments aimed to thoroughly assess the performance of these new MMMs, studying in detail the significance of the dispersion of these porous fillers, including their influence on the aging phenomenon.

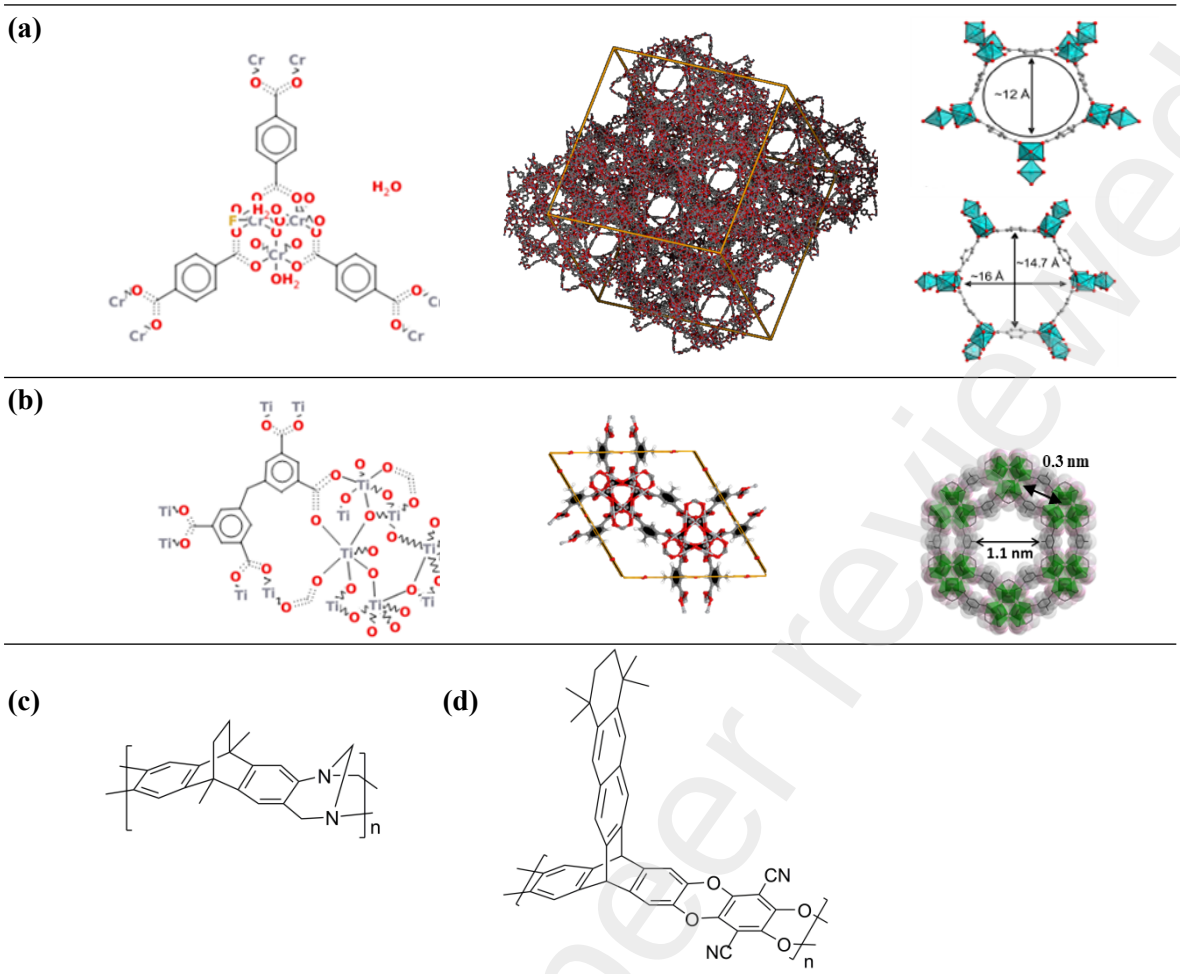


**Fig. 1** (a) MIL-101(Cr) with the single unit, its framework cell, hexagonal and pentagonal cavities [46]; (b) MIL-177(Ti) with the single unit, its framework cell, hexagonal cavities and smallest narrow channels [44]; structures of polymers PIM-EA-TB (c) and PIM-TMN-Trip (d).

## 2 Experimental

### 2.1 *Materials*

All starting materials and solvents were purchased from Sigma-Aldrich and were used as received without further purification. Gases were supplied by Sapio at a minimum purity of 99.9995%.

***MIL-101(Cr):***

MIL-101(Cr) was synthetized following a microwave assisted hydrothermal synthesis, as previously reported [46]. The obtained nanoparticles were kept in $CHCl_3$ to avoid their aggregation and facilitate their dispersion with the polymers.

***MIL-177(Ti):***

MIL-177(Ti) was synthesized by refluxing a mixture of $Ti(iPrO)_4$ and 5,5'-methylenediisophthalic acid ($H_4$mdip) in formic acid under ambient pressure, as described previously [44]. The MOFs were kept in $CHCl_3$ to avoid aggregation and facilitate their dispersion with the polymers.

### 2.2 *PIMs synthesis*

PIM-EA-TB was synthesized from 9,10-dimethyl-2,6(7)-diamino-9,10-ethanoanthracene (Fig. 1c). The ethanoanthracene (EA) units are linked by Tröger's base, and the synthesis was described in previous works [16,47]. PIM-TMN-Trip was produced using a monomer based on triptycene that contains a fused tetramethyltetrahydronaphthalene (TMN) unit as described previously [17] (Fig. 1d).

### 2.3 *Membrane preparation and conditioning*

All the pristine PIM and MMM films were cast from chloroform solutions. The PIM/filler weight ratios were 9:1 and 7.5:2.5, corresponding to filler weight percentages of 10 wt% and 25 wt%, respectively. In a typical experiment (10 wt% and 25 wt% loading), a dispersion of the filler in $CHCl_3$ (i.e., 70 mg in 6 mL of $CHCl_3$) was sonicated for 1 h, it was then poured into a flask containing the PIM solution (i.e., 700 mg in 12 mL of $CHCl_3$) and then sonicated for a further 1 h. The final dispersion was poured onto a Petri dish, covered with a glass lid and the $CHCl_3$ allowed to slowly evaporate for three days, until the film was easily peeled off. This procedure yielded robust, self-standing films for all the reported MMMs. Methanol treatment, essential to remove the last traces of casting solvent, consisted in soaking the membrane for 24 h in anhydrous methanol, followed by drying for 24 h at 25 °C and ambient pressure. The thermal conditioning was carried out in a vacuum oven, at 140 °C for 24 h. Membranes for aging studies were kept at ambient conditions, without any control of humidity or air exposure.

### 2.4 *MOFs characterizations*

Powder X-ray diffraction (PXRD) data were collected on a Panalytical X'Pert Pro Diffractometer Model PW3040/60 using CuKα (λ= 1.5406 Å) radiation at an operating voltage of 40 kV and 30 mA at room temperature. A small amount of dry crushed powder was put onto the sample holder and scanned over the angular range of 2-30° (2θ). Scanning electron microscopy (SEM) was undertaken using a FEI Quanta 200 ESEM. For powder samples, the powder was scattered onto a carbon disc. Then coated with platinum by sputtering using an Emitech coater. Nitrogen adsorption measurements were carried out using a Micromeritics ASAP 2020 sorption analyser. The samples were first outgassed at 150 °C for 16 h under high

vacuum. After cooling, degassed samples were reweighed and placed in the analysis port, then manually outgassed for 2 h. Nitrogen adsorption/desorption isotherms were recorded at 77 K and the BET surface areas were calculated from $N_2$ adsorption data by multi-point Brunauer-Emmet-Teller (BET) analysis. The free space of the sample tube was measured after analysis.

### 2.5 *Membranes characterization*

Membranes were characterized by scanning electron microscopy (SEM) (Phenom Pro X desktop SEM). The samples for cross-section SEM characterization were prepared by freeze-fracturing in liquid nitrogen. Samples were analysed without sputter-coating with gold. Elemental analysis and mapping analysis were performed with the Phenom Pro X desktop SEM, which is equipped with an energy dispersive X-ray spectroscopy detector (EDX) and a Phenom Elemental Mapping Software.

### 2.6 *Permeability measurements*

Single gas permeation tests were carried out at 35 °C and at a feed pressure of 1 bar, using a fixed-volume pressure increase instrument constructed by EESR following the design of HZG, and described elsewhere [48]. Permeability coefficients ($P$), and diffusion coefficients ($D$), were determined by the time-lag method [49]. The apparent solubility, $S$, was indirectly calculated assuming the validity of the solution diffusion model as $S = P/D$. The ideal selectivity for a pair of gases is the ratio of the permeability of the two species, $\alpha_{(A/B)} = P_A/P_B$.

Mixed gas permeation tests were carried out using a custom made constant pressure/variable volume instrument, described elsewhere [50], equipped with a quadrupole mass filter (HPR-20 QIC Benchtop residual gas analysis system, Hiden Analytical). Model mixtures of air, flue gas and biogas were prepared by mixing the pure gases with electronic mass flow controllers in the ratios $N_2/O_2$ (80/20 vol%), $CO_2/N_2$ (15/85 vol%) and $CO_2CH_4$ (35/65 vol%), respectively.

## 3 Results and discussion

### 3.1 *Chemical and Morphological characterization of MOFs: MIL-101(Cr) and MIL-177(Ti)*

The structures of MIL-101(Cr) and MIL-177(Ti) are schematically shown in Fig. 1a and Fig. 1b, respectively. MIL-101(Cr) is a chromium terephthalate-based MOF with a cubic zeotype, built up from hybrid supertetrahedra (ST) of chromium trimers connected through terephthalate

linkers. It forms two distinct mesoporous cages with free internal diameters of 2.9 nm and 3.4 nm [46]. MIL-177(Ti) is a porous 3D mdip-based Ti-MOF composed of a $Ti_{12}O_{15}$ cluster secondary building unit (SBU), with a honeycomb crystal packing that features nanosized pores. Adjacent SBUs are linked by both formate ions and mdip linkers and each ligand connects four Ti-oxoclusters. The resulting 3D arrangement features large (ca. 1.1 nm) and accessible hexagonal channels that run along the *c*-axis, along with narrower channels (ca. 0.3 nm) along the *a–b* plane [44]. The powder X-ray diffraction patterns for both MOFs are shown in Fig. 2a-b, which show high crystallinity and purity that are in line with previously reported examples [44,46]. Scanning electron microscopy (SEM) shows a predominantly octahedral morphology for MIL-101(Cr) (Fig. 2c), which is expected for such a cubic crystal system, while for MIL-177(Ti) shows a hexagonal morphology (Fig. 2d). Fig. 2c shows that the average particle size of MIL-101(Cr) falls within ca. 20-70 nm, while the average MIL-177(Ti) is found around 100-200 nm (Fig. 2d). $N_2$ sorption isotherms at 77 K of crystalline MIL-101(Cr) and MIL-177(Ti) demonstrates a high uptake at very low relative pressures (Fig. 2e-f) that is typical of highly microporous materials, as defined by IUPAC [2]. The Brunauer-Emmett-Teller surface areas (BET, Table 1) suggests that MIL-101(Cr) is significantly more porous than MIL-177(Ti), with values of ~3270 $m^2g^{-1}$ that lie within the typical range reported before [46,51,52], whereas MIL-177(Ti) has a BET of only 600 $m^2g^{-1}$which is also lower than those of the two matrix polymers, (PIM-EA-TB = 1028 $m^2g^{-1}$; PIM-TMN-Trip = 1034 $m^2g$-$^1$).

Table 1. Measured BET surface area, Fractional Free Volume (FFV), density, average particle size of the MOFs and the PIMs used in this work.

| Materials | BET surface area, ($m^2$ $g^{-1}$) | FFV (%) | Density (g $cm^{-1}$) | Av. Size (nm) | Ref. |
|---|---|---|---|---|---|
| MIL-101(Cr) | 3270 | | 0.44 | 20-70 | **This work** |
| MIL-177(Ti) | 600 | | - | 100-200 | **This work** |
| **PIM-EA--TB** | 1028 | 27.6 | 1.03 | | [16] |
| **PIM-TMN-Trip** | 1034 | 31.4 | 0.965 | | [17] |

### 3.2 *The "matrix" polymers: PIM-EA-TB and PIM-TMN-Trip*

PIM-EA-TB (Fig. 1c) [16] is derived from an ethanoanthracene diamine moiety that underwent polymerization via Tröger's base formation. The rigid bridged bicyclic TB linking unit is attractive due to the combination of its V-shape, which confers additional contortion, coupled with two basic nitrogen which provides affinity for slightly Lewis acidic gases, such as $CO_2$. PIM-EA-TB has been exploited in for applications such as desalination[53], catalysis[54], electrochemistry [55] and gas separation [56]. PIM-TMN-Trip (Fig. 1d) [17] was synthesised

via the well-established nucleophilic aromatic substitution of bis-catechol moieties (in this case the benzotriptycene) with tetra-fluorinated monomers, which is typical of the archetypal PIM-1[57]. These extended triptycene structural units provided the first examples of "ultra-permeable" PIMs, which have redefined the Robeson upper limits for $CO_2$ based gas pairs [21].

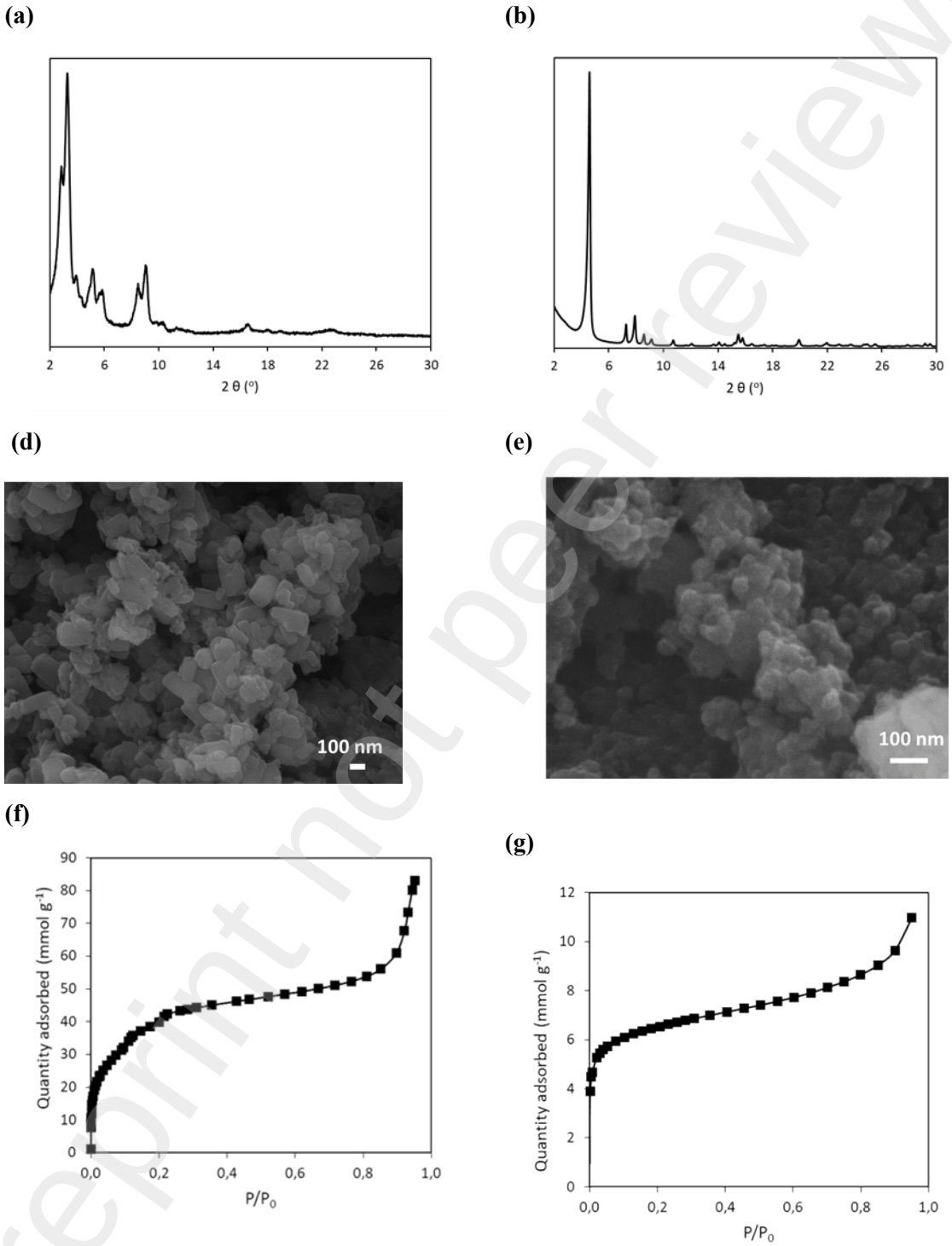


**Fig. 2** (a-b) X-ray powder diffraction patterns, (c-d) SEM images, (e-f) 77 K $N_2$ sorption isotherms, of MIL-101(Cr) on the left and for MIL-177(Ti) on the right.

### 3.3 *Chemical and Morphological characterization of the MMMs*

All MMMs were obtained by sonicating a dispersion of the MOF in chloroform and pouring the appropriate amount into a chloroform solution of the matrix polymer. After casting the solution in a Petri dish and subsequent evaporation of the solvent, visually homogenous films were obtained (Fig. 3a).

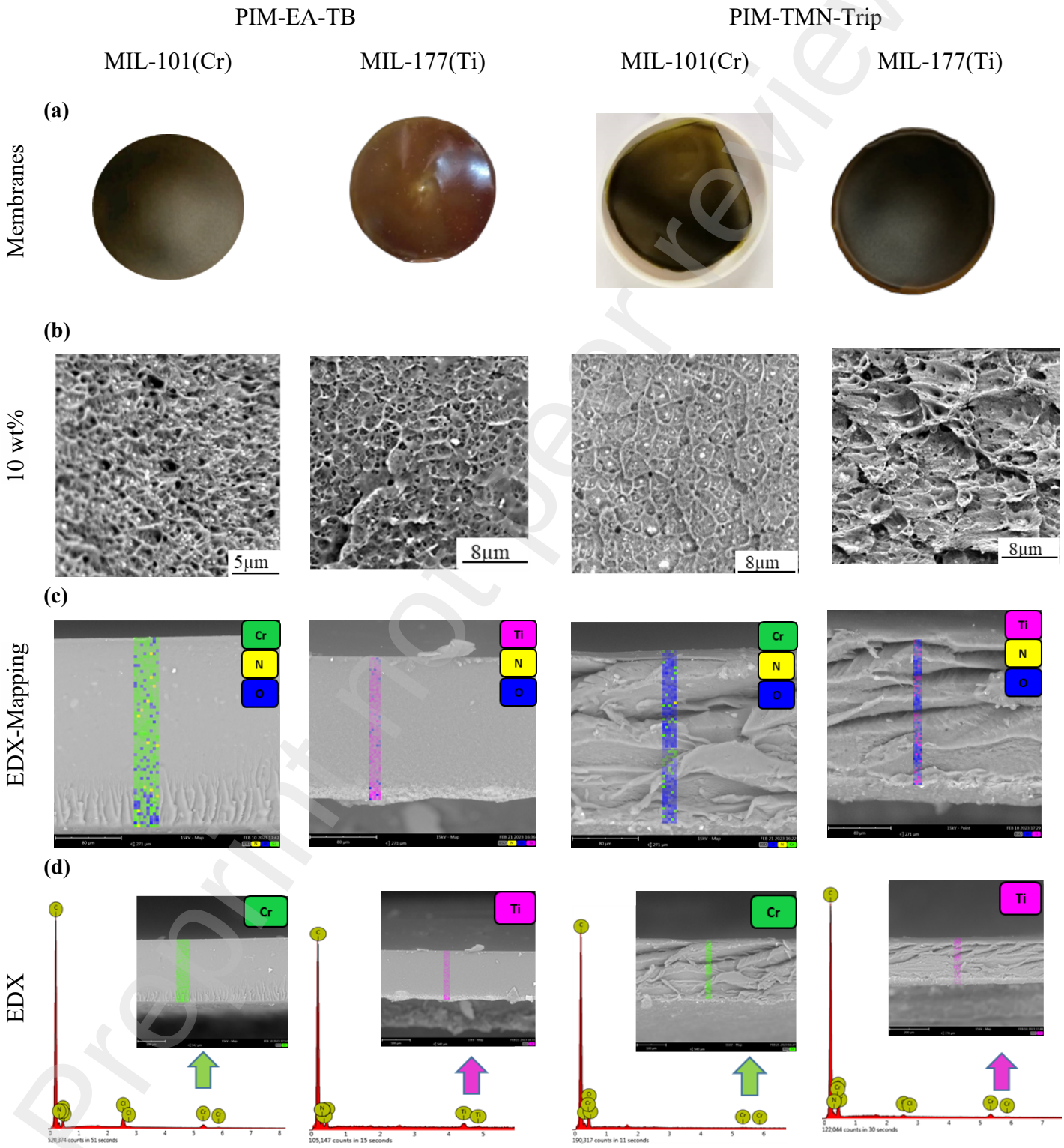

**Fig. 3** (a) Films of MMMs. (b) SEM images of the MMMs at a magnification of 10,000× and an accelerating voltage of 10 kV. (c) Mapping and (d) EDX of the cross-section at magnification 500× and 1000× at an electron acceleration voltage of 15 kV for the MMMs made of PIM-EA-TB or PIM-TMN-Trip, with MIL-101(Cr) or MIL-177(Ti), respectively.

Scanning Electron Microscopy (SEM) and Energy-dispersive X-ray (EDX) mapping of the cross-section of the MMMs revealed a good dispersion of the MOFs within the PIM matrix (Fig. 3d), with smaller network dimensions for MIL-10(Cr), which is in accord with its smaller particle size (20-70 nm) compared to MIL-177(Ti) (between 100-200 nm) (Fig. 2c-d). Mapping and EDX clearly demonstrated the homogeneous dispersion over the entire thickness of the membranes (Fig. 3c-d). The presence of oxygen is more evident in MMMs based on PIM-TMN-Trip compared to PIM-EA-TB, which is not surprising considering the presence of the dioxane rings in the polymer's backbone of the former. Moreover, in some as-cast membranes (i.e., prior methanol treatment), the EDX analysis clearly shown chlorine peaks, which are attributed to residual chloroform casting solvent (Fig. 3d). This explains the main reasons why the alcohol treatment is essential for PIMs, as the presence of residual casting solvent blocks the diffusion of gases resulting in the underestimation of the permeability [37].

### 3.4 *Single gas transport properties comparison between different MMMs and pristine PIMs*

Single gas permeation data were measured for all the MMMs at 35 °C following the order He, $H_2$, $O_2$, $N_2$, $CH_4$ and $CO_2$. Detailed results of permeability, diffusivity and solubility are given in the supporting information (Table S1-S4).

#### *3.4.1 PIM-EA-TB gas transport properties as function of MOF concentration*

The loading of MIL-101(Cr), from 0-25 wt%, produces a general increase of the permeability for PIM-EA-TB (Fig. 4a). As anticipated, the higher permeability can be attributable to the impact of the MOF's large cavities, which can provide a preferential pathway for gas diffusion. The presence of pore windows of a well-defined size may help with fine-tuning of the selectivity, especially for gas pairs with a large difference in kinetic diameters, such as $H_2/N_2$, $H_2/CH_4$ and $He/N_2$ (Fig. 4c), alternatively the MOF may help to rigidify the PIM matrix resulting in higher selectivity. On the other hand, the dispersion of MIL-177(Ti) in PIM-EA-TB produced a very modest increase in permeability compared to the neat polymer for He and $H_2$, and a weak decrease in permeability for gases with larger diameters ($CO_2$, $O_2$, $CH_4$, and $O_2$). The increased size-sieving character upon addition of the MOFs in PIM-EA-TB is

confirmed by the steeper correlation of gas diffusion as function of gas diameters (Fig.S 3). For this reason, the relative selectivity for all gas pairs including He and $H_2$, was found to increase (Fig. 4f).

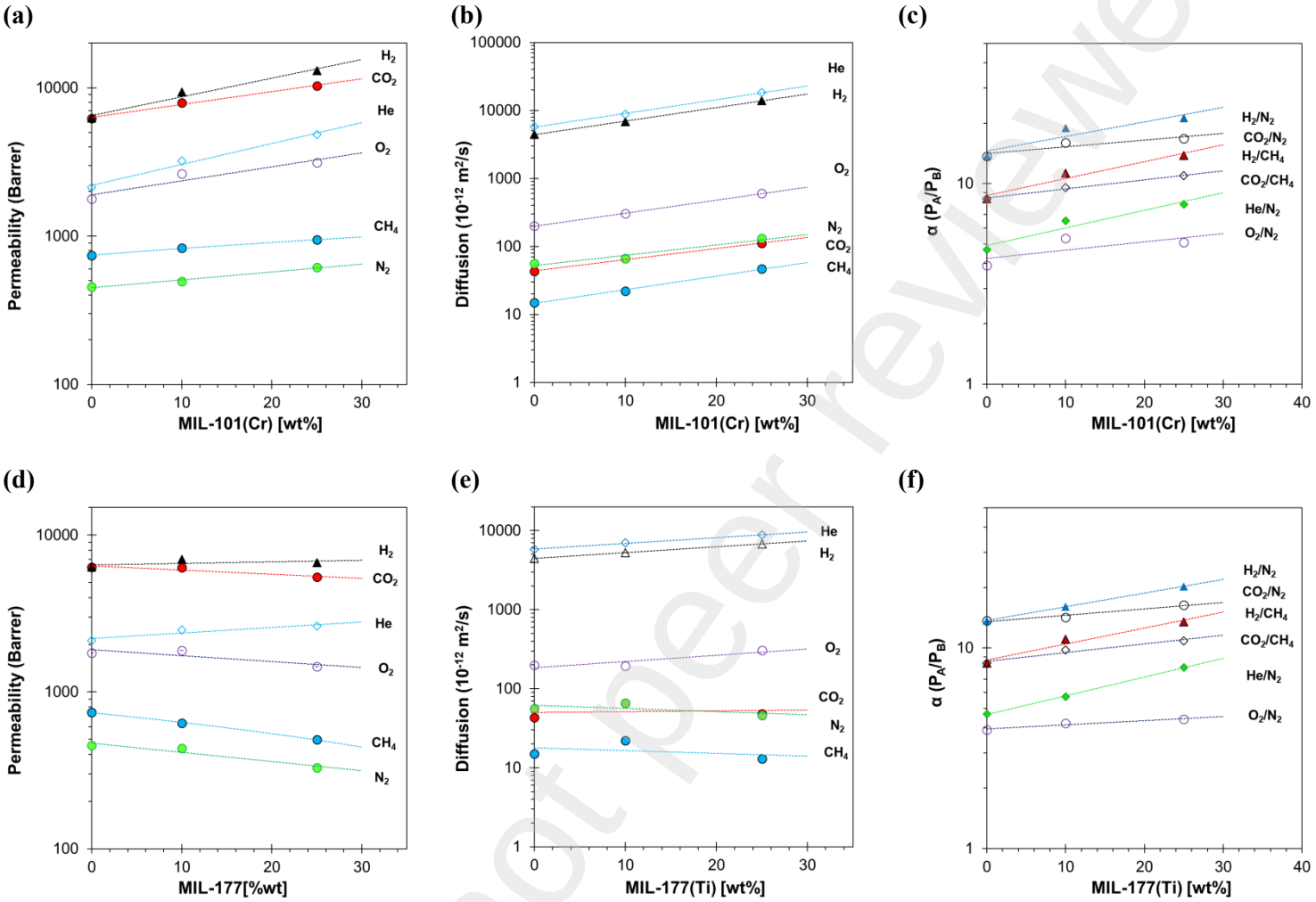


**Fig. 4** Gas permeability, diffusion coefficient and permeability selectivity as function of MOF concentration (0 wt%, 10 wt%, and 25 wt%) for freshly MeOH treated PIM-EA-TB/MIL-101(Cr) MMMs (a, b, c) and for PIM-EA-TB/MIL-177(Ti) (d, e, f).

### *3.4.2 PIM-TMN-Trip gas transport properties as function of MOF concentration*

The dispersion of 10wt% MIL-101(Cr) in the ultrapermeable PIM-TMN-Trip polymer led to a slight decrease in the permeability for all gases, except for $H_2$ and He (Fig. 5a). Consequently, we noted an increase in the selectivity for $H_2/N_2$, $He/N_2$, followed by $H_2/CH_4$, $O_2/N_2$, $CO_2/CH_4$ and $CO_2/N_2$ (Fig. 5c). A similar but more pronounced effect was observed when MIL-177(Ti) (100-200 nm) was dispersed into PIM-TMN-Trip, (Fig. 5d) enhanced the overall selectivities, especially evident for gas pairs such as $H_2/CH_4$, $H_2/N_2$ and $He/N_2$ (Fig. 5f). In addition, He and $O_2$ showed a reverse order of permeation in the presence of MIL-177(Ti) ($He>O_2$) compared

279 to the pristine PIM-TMN-Trip ($O_2$>He), evidencing a greater preference for the transport of
280 smaller gases.

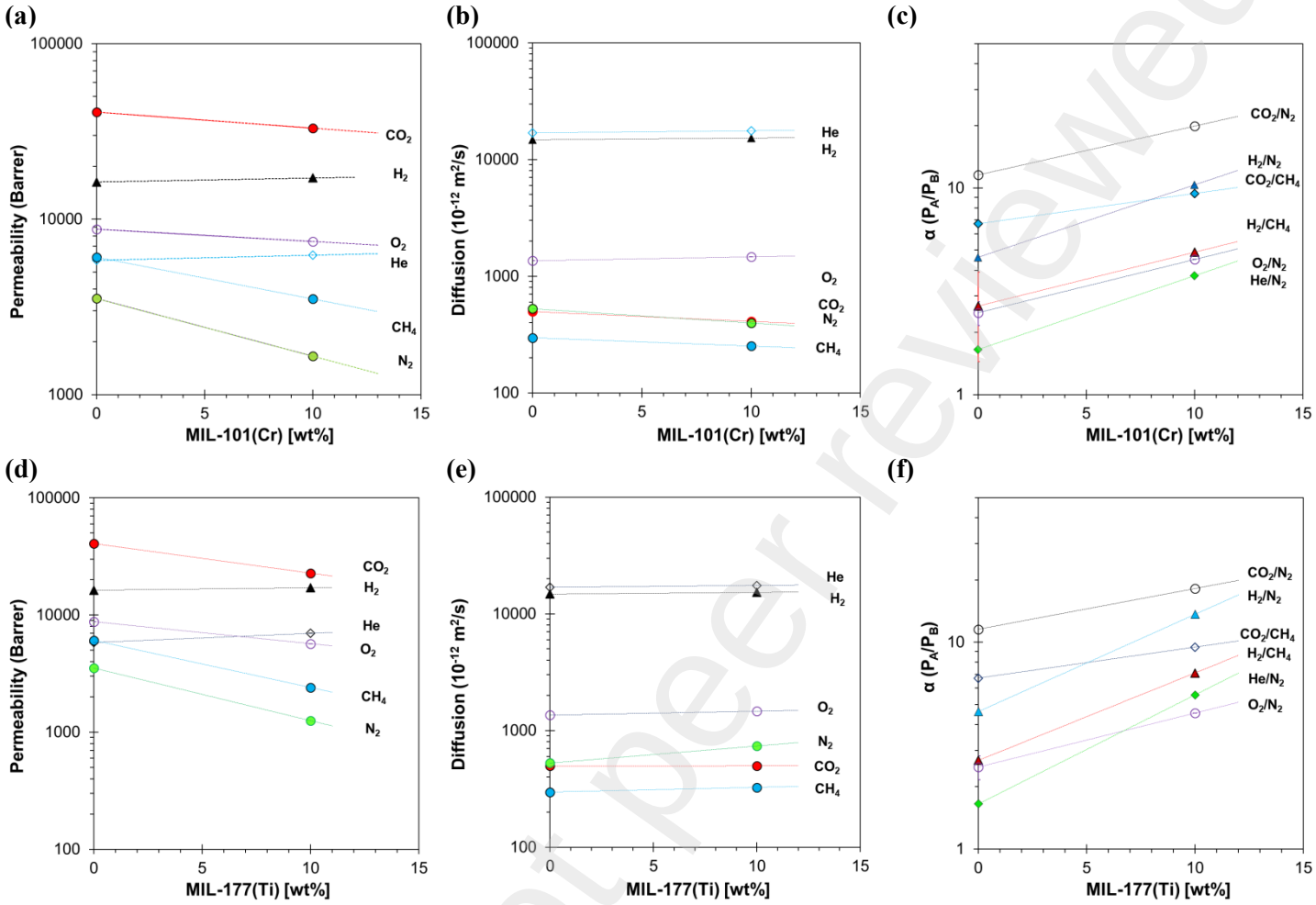


**Fig. 5** Gas permeability, diffusion coefficient and selectivity as function of MOF concentration (0 wt% and 10 wt%) for freshly MeOH treated (a, b, c) PIM-TMN-Trip/MIL-101(Cr) and (d, e, f) PIM-TMN-Trip/MIL-177(Ti) membranes.

281

282 Comparing the gas transport properties across all reported MMMs emphasises the distinctive
283 impact of the combination of MOFs with selected polymers, which results in a unique
284 enhancement of the gas transport properties of the MMMs. The addition of the fillers
285 influenced PIM-EA-TB with the creation of additional free volume, resulting in the increase of
286 the permeability for several gases. On the other hand, the incorporation of MOFs into the
287 ultrapermeable PIM-TMN-Trip produced a general reduction of the gas permeability, changing
288 the bulk properties of the neat polymer by occupying its free space, and resulting in an increase
289 of selectivities.

### 3.5 *Influence of the sample conditioning on the transport properties: methanol treatment and thermal conditioning*

Analysis of permeability for all of the MMMs under different treatments were performed to understand the dependence of gas transport properties on both sample conditioning and aging time. Single gas permeation tests were carried out at the standard temperature of 35 °C after methanol treatment which, as anticipated, is a crucial step to remove the residue of casting solvent. Subsequently, the membrane was subjected to thermal treatment at 140 °C, which is known to accelerate initial aging while stabilising the performance. Finally, re-analysis was carried out after a long period of natural aging (approximately 5 years). For a more quantitative evaluation of the effect of the filler and the sample treatment, the gas permeability of the MMMs was assessed using the Maxwell model, which is one of the most commonly used models to describes the effective permeability of a gas species in MMMs [58–61]. It expresses the effective permeability as a function of the permeability of the polymer matrix and that of the filler [62]:

$$P_{MMM} = P_c\left|\frac{P_d + 2P_c - 2\Phi_d(P_c - P_d)}{P_d + 2P_c + \Phi_d(P_c - P_d)}\right| \quad \text{(Eq. 1)}$$

where the $P_{MMM}$ is the effective permeability of the mixed matrix membrane, $P_c$ and $P_d$ are the gas permeabilities of the continuous phase (polymer matrix) and the dispersed phase (MOF), respectively, and $\Phi_d$ is the volume fraction of the dispersed phase. The results were compared with the two possible extreme cases: 1) the permeability of the dispersed phase ($P_d$) is much lower compared to the pristine polymer ($P_d << P_c$) and 2) the dispersed phase has a much higher permeability than the neat polymer ($P_d >> P_c$) [37,40,63,64]. A more detailed discussion of the Maxwell model is reported in the SI.

#### *3.5.1 Application of Maxwell model to PIM-EA-TB based MMMs*

Fig. 6a shows that $CO_2$ permeability of membranes based on MIL-177(Ti) in PIM-EA-TB tends towards the lower limit of the Maxwell model ($P_d << P_c$), which suggests that MIL-177(Ti), with its narrow windows of about 3.0 Å, obstructs the passage of $CO_2$ (which has a diameter of 3.02 Å) [65] as well the passage of $CH_4$ and $N_2$ (3.18 Å and 3.04 Å respectively) consistent with the prediction of Maxwell model for low values. On the other hand, MIL-177(Ti) favouring the passage of $H_2$ and He, plots the permeability according to the predicted values falling in the middle of Maxwell window (See SI Fig.S 1). It can be easily observed that $CO_2$ deviation, from the lower limit towards permeable region, is higher than those of $CH_4$ and the deviation becomes more significant with the decrease of gas diameter ($O_2 > CO_2 > N_2 > CH_4$;

2.89Å> 3.02Å>3.04Å>3.18 Å). Thus implies that the gas transport performance is influenced by the presence of MOF's cavities with well-defined size (3 Å) and not by formation of voids at interface. The membranes containing MIL-177(Ti) also show a considerable reduction of $CO_2$ permeability upon thermal treatment for all MOF concentrations, neat polymer included. This indicates that the system was not able to compensate for the reduction of free volume of the neat polymer after the accelerated aging induced by the high temperature.

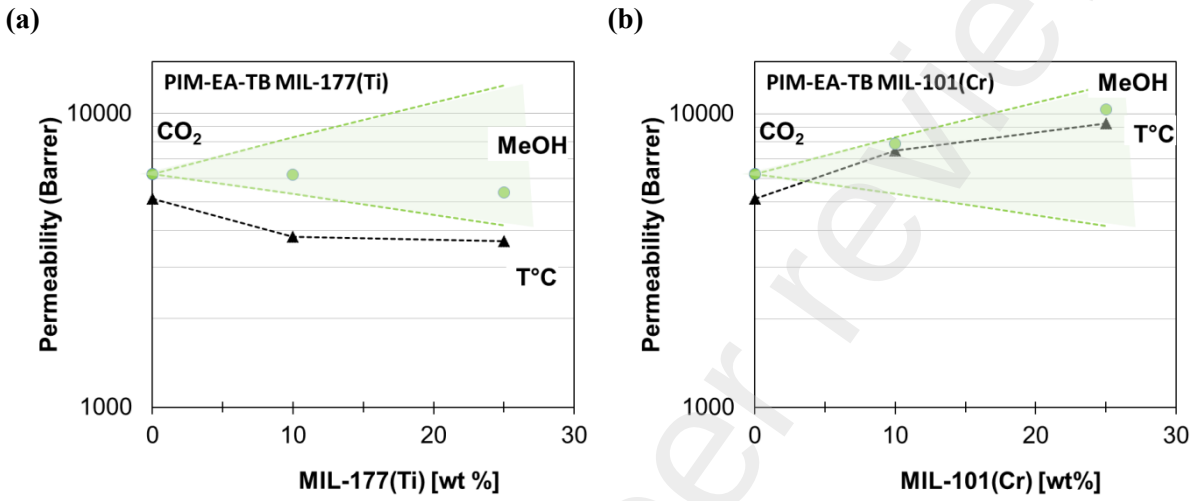


**Fig. 6** Different trends of $CO_2$ permeability as function of (a) the MIL-177(Ti) and (b) MIL-101(Cr) content in PIM-EA-TB after MeOH treatment (○; MeOH) and thermal conditioning at 140 °C (△). The two green dashed lines represent the upper limit ($Pd=\infty$) and lower limit ($Pd=0$) of the Maxwell model [40].

Conversely, the $CO_2$ permeability of PIM-EA-TB/MIL-101(Cr) MMMs is consistent with the prediction made by the Maxwell model for highly permeable fillers, showing a permeability close to the upper limit ($P_d>>P_c$) for MeOH treated membranes, with only a slight reduction upon thermal treatment (the same was observed for other gases See SI Fig.S 1). This means that MIL-101(Cr) not only boosts the permeability of the membrane compared to the pristine polymer, but it also retains better the high permeability after thermal treatment (Fig. 6b). This positive effect may be ascribed to the ability of MIL-101(Cr) to prevent the collapse of the large free volume elements of PIM-EA-TB upon thermal conditioning, but also to the intrinsic high permeability of MIL-101(Cr) itself.

### *3.5.2 Application of Maxwell model to PIM-TMN-Trip based MMMs*

PIM-TMN-Trip-based MMMs showed a $CO_2$ permeability below the lower limit of the Maxwell window ($P_d<<P_c$) (Fig. 7a), implying that the data are not consistent with the predictions of this model. This can be attributed to the alteration of the bulk properties of the

polymer matrix by the fillers. The MOFs seem to affect the packing of the polymer chains by occupying a part of the free volume of the PIM-TMN-Trip or by a change of the polymer dynamics and a net stiffening, or both. This is especially evident for MIL-177(Ti), which possesses higher particle dimensions (100-200 nm) compared to MIL-101(Cr) (20-70nm) and where the thermal treatment produces a drastic decrease in permeability (Fig. 7a). The permeability reduction during accelerated aging at 140°C is similar for MMMs containing both MOFs, but is more pronounced in PIM-TMN-Trip than in PIM-EA-TB. Summarizing, the Maxwell analysis suggests that the larger free volume of PIM-TMN-Trip is more adversely influenced by the presence of filler particles than PIM-EA-TB. For the latter it appears that the MOFs serve as size-selective particles favouring the permeation of smaller $H_2$ and He, which show permeabilities in good accordance with those predicted by Maxwell model (for other gases see SI Fig.S 2), therefore, having a positive effect on selectivity for several gas pairs.

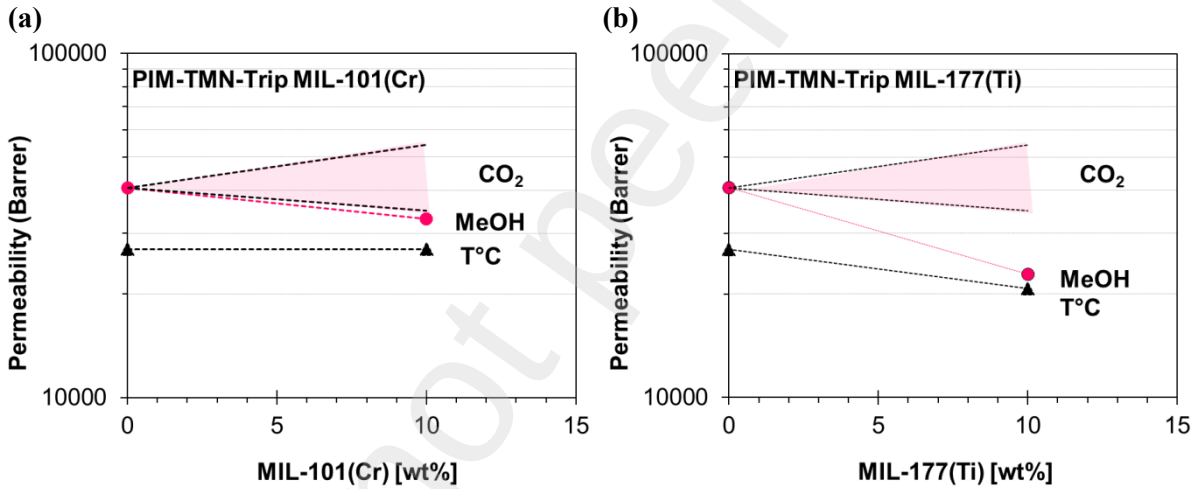


**Fig. 7** Trends in $CO_2$ permeability as a function of the MIL-101(Cr) content and the MIL-177(Ti) content in PIM-TMN-Trip based MMMs after MeOH treatment ( ●, MeOH) and thermal conditioning at 140 °C ( ▲). The dashed purple lines represent the upper limit ($Pd=\infty$) and lower limit ($Pd=0$) of the Maxwell equation [40].

### 3.6 *Investigation of natural physical aging*

It is known that PIMs undergo a physical aging, which reduces the internal free volume [23]. To test any improvements due to the incorporation of the MOF fillers, gas permeation tests were performed on the membranes after prolonged natural aging (Fig. 8a and Fig. 8b).

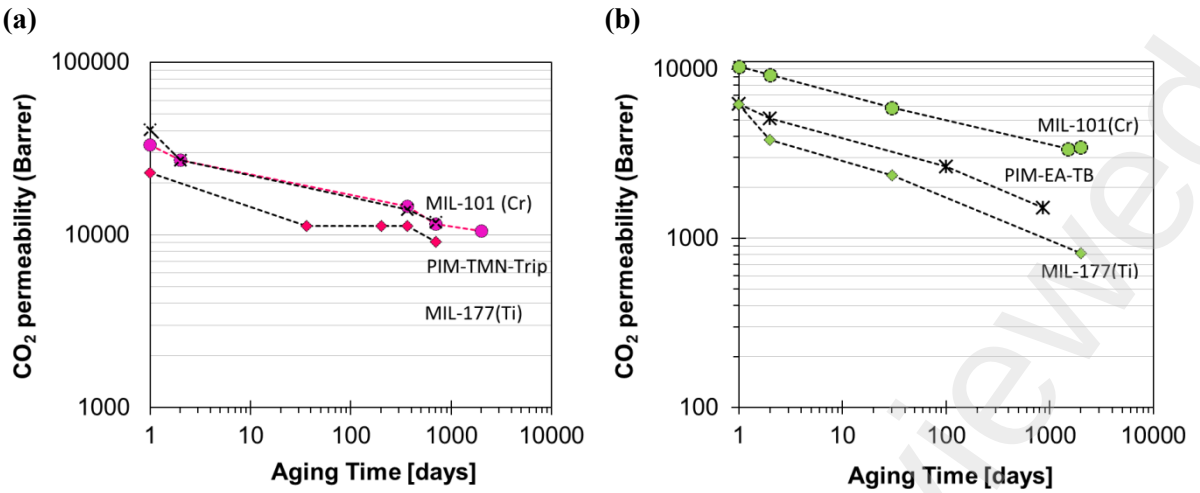


**Fig. 8** Change in $CO_2$ permeability over time for: (a) neat PIM-TMN-Trip (×) and (b) neat PIM-EA($Me_2$)-TB (⁎) for both with MIL-101(Cr) (●) and MIL-177(Ti) (◆)

360

361 **Fig. 8**A shows the changes in $CO_2$ permeability over an extended ageing period, for pristine
362 PIM-TMN-Trip and PIM-EA-TB, and for their corresponding MOFs based MMMs. The
363 results suggest that MIL-101(Cr) neither affect the $CO_2$ permeability of neat PIM-TMN-Trip,
364 nor does it contribute to mitigating the loss of free volume compared to the neat polymer (Fig.
365 8a). This behaviour is attributed to the extremely high initial free volume of PIM-TMN-Trip,
366 which is less likely to be affected by the presence of a porous filler such as MIL-101(Cr) and
367 MIL-177(Ti). The same effect was observed for the dispersion of the smaller MIL-177(Ti) into
368 the PIM-EA-TB. On the other hand, the MMM formed by the combination of PIM-EA-TB and
369 MIL-101(Cr) shows an initial increase of the $CO_2$ permeability that is maintained for over 2000
370 days with the reduction of $CO_2$ permeability at the same rate for this MMM as for the pristine
371 polymer. These results demonstrate the positive effect that the incorporation of MIL-101(Cr)
372 has for enhancing gas permeability for MMMs based on this polymer even with extended
373 aging.

374 3.7 *Mixed gases transport properties*

375 Due to their impressive results using single gases, mixed gas permeation measurements for the
376 MMMs containing MIL-101(Cr) were performed for three important gas separations, namely
377 biogas upgrading ($CO_2/CH_4$), $CO_2$ capture from flue gas ($CO_2/N_2$) and oxygen/nitrogen
378 enrichment of air ($O_2/N_2$) (Fig. 9).

379

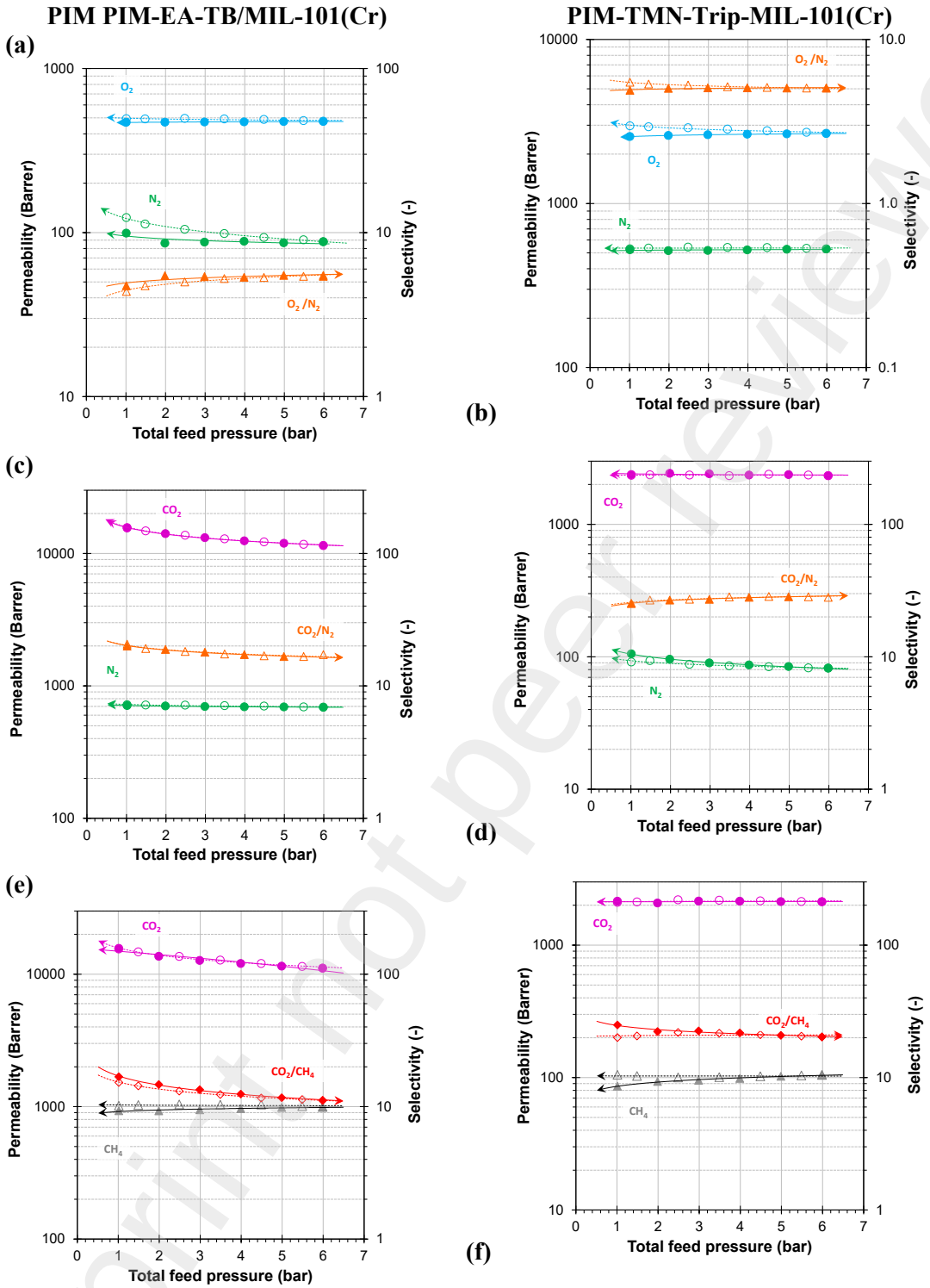


**Fig. 9** (a-b) Pressure dependence of $O_2$ and $N_2$ permeabilities and $O_2/N_2$ selectivity in binary mixture conditions for $O_2/N_2$ (20:80 vol%); (c-d) Pressure dependence of $CO_2$ and $N_2$ permeabilities and $CO_2/N_2$ selectivity in binary mixture conditions for $CO_2/N_2$ (15:85 vol%); (e-f) Pressure dependence of $CO_2$ and $CH_4$ permeabilities and $CO_2/CH_4$ selectivity using the binary $CO_2/CH_4$ (35:65 vol%) mixture for the PIM-EA-TB/MIL-101(Cr) and PIM-TMN-Trip/MIL-101(Cr) aged for 2000 days. Closed symbols for stepwise increase of the pressure and open symbols for the subsequent stepwise decrease of the pressure.

381

Measurements were performed under pressures ranging from 1 to 6 bar(a). PIM-EA-TB/MIL-101(Cr) showing a gentle decrease of $CO_2$ permeability as a function of increased feed pressure typical of dual-mode behaviour observed for $CO_2/CH_4$ (Fig. 9e) and $CO_2/N_2$ mixtures (Fig. 9c). This also causes a simultaneous decrease of $CO_2/CH_4$ and $CO_2/N_2$ selectivity. Interestingly, we noticed some hysteresis of $CO_2$ and $CH_4$ permeability when the pressure is reduced back to 1 atm after the initial pressure increase. This can be attributed to a slight $CO_2$-induced dilation of the polymer (swelling), which induces the formation of a larger amount of free volume in the polymer matrix, which remains when the pressure is decreased. This leads to a higher $CH_4$ permeability and a slightly lower selectivity. In the separation of the $CO_2/N_2$ mixture no hysteresis is noticed, most likely due to the lower partial pressure of $CO_2$. For the $O_2/N_2$ separation, the $O_2$ permeation appears pressure-independent while the permeation of $N_2$ decreases as a function of the pressure (Fig. 9a). This suggests a strong size sieving character of MIL-101(Cr), when loaded into PIM-EA-TB, which in the presence of real mixtures facilitates the passages of smaller molecules like $O_2$ whilst hampering the permeation of $N_2$ and $CO_2$, especially at high pressure. MMMs based on the system PIM-TMN-Trip/MIL-101(Cr) show very little pressure dependence for both permeability and selectivity for all measured gas mixtures (Fig. 9b-d-f).

### 3.8 *Performance overview*

Fig. 10 gives a complete overview of gas permeability and selectivity of all MMMs, and for their corresponding pristine polymers, after methanol and natural aging conditioning.

Almost all methanol-treated MMMs showed high permeability and modest selectivity generally moving data towards the right-hand side of the Robeson plots relative to the data for the polymer. This suggests that the polymer matrix still provides the main resistance to transport, while the fillers offer a preferential diffusion pathway. After MeOH treatment, all MMMs based on PIM-EA-TB (green circle open symbols), exhibit an increased selectivity compared to the neat polymer (green circle filled symbol), with a further increase in permeability for MIL-101(Cr) (Fig. 10 left column). On the other hand, MIL-177(Ti) shows a slight increase in permeability only for the small $H_2$ (Fig.8 right column). Almost all MeOH MMMs based on PIM-TMN-Trip (violet open circle symbol) show an increased selectivity for both MOFs, although at expenses of their permeability.

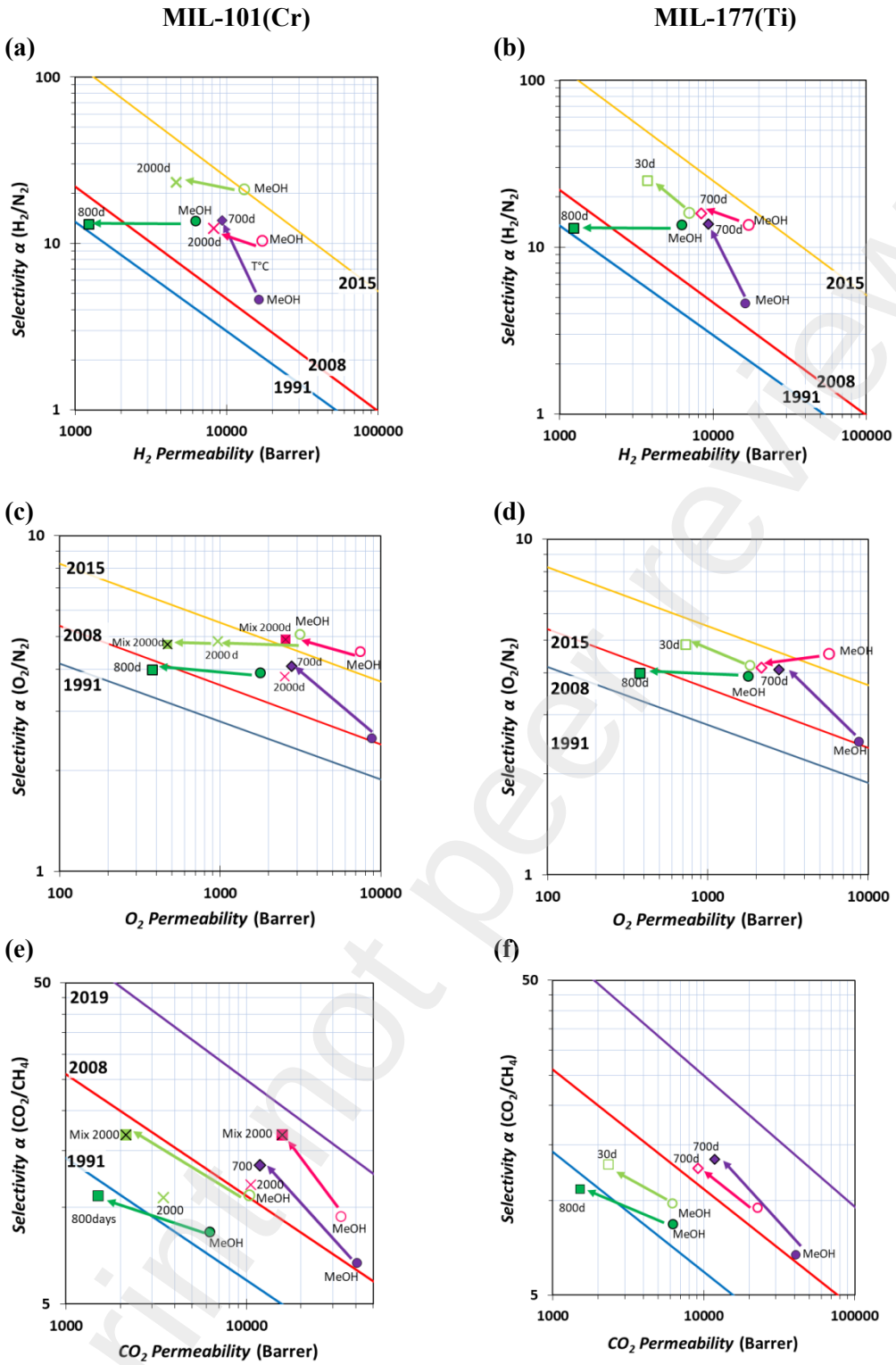


**Fig. 10** Robeson's plots for $H_2/N_2$, $O_2/N_2$, $CO_2/CH_4$ gas pairs, showing the data for methanol (● circle), aging (■ square) and extended aging (◆ diamond) for neat PIM-EA-TB (green filled symbols), neat PIM-TMN-Trip (violet filled symbols) and for respectively MMMs (open symbols). The × open symbol and ⊤filled symbol are the data for 2000 aging single and under mixed gas, respectively for MMMs. The arrows serve as a guide to the eye for following the typical effect of aging. Blue line 1991 upper bound, red line 2008 upper bound ; yellow line 2015; violet line 2019 upper bound [9,21,66,67]

For the $H_2/N_2$ gas pair, a good compromise between permeability and selectivity was achieved using PIM-TMN-Trip with MIL-177(Ti), resulting in an increase in selectivity from 4 to 10, coupled with a small increase in $P_{H_2}$ permeability (from ~ 16000 to 17000 Barrer), approaching the 2015 upper bound (Fig. 10b). The performance remains consistent even after 700 days of aging, with an increase in selectivity and a decrease in permeability ($P_{H_2}$ ~8300; $\alpha_{H_2/N_2}$ = 16). This performance is within the range of TPIM-2/PAF MMMs, one of the best performing MMM for $H_2/N_2$ separation reported so far ($P_{H_2}$ ~ 4800; $\alpha_{H_2/N_2}$ = 27)[68], but with twice the hydrogen permeability, while maintaining selectivity. PIM-EA-TB/MIL-101 also exhibits an excellent trade-off between permeability and selectivity, with an increase in selectivity from 14 to 21 and a remarkable increase $P_{H_2}$ from ~ 6000 to 13000 Barrer, which approaches the 2015 upper bound (Fig. 10a). This further improves after 2000 days of aging, following the typical aging behaviour with a reduction in permeability compensated by an increase in selectivity ($P_{H_2}$ ~4600; $\alpha_{H_2/N_2}$ = 23).

For the $O_2/N_2$ gas pair, the best initial performance was obtained for PIM-TMN-Trip in combination with both fillers, with a modest reduction of the $O_2$ permeability (from ~ 9000 to 7000 for MIL-101(Cr) and from 9000 to ~ 6000 Barrer for MIL-177(Ti)), compensated by a significant two-fold increase of selectivity (from 2.5 to 4.5), which produced data that surpassed the 2015 upper bound (Fig. 10c-d, pink open circle). The long aging resulted in a slight reduction of both permeability and selectivity, mirroring the aging behaviour of the neat polymer. Conversely, the MIL-101(Cr) into PIM-EA-TB showed an increase in $O_2$ permeability compared to the neat polymer (from ~ 1700 to 3000), with a further increase in $O_2/N_2$ selectivity (from 4 to 5), surpassing the 2015 upper bound. This MMM demonstrate less pronounced aging relative to the pristine polymer (Fig. 10c, green symbols), as even after 2000 days of aging it still outperformed the neat polymer aged for 800 days, even when exposed to a mixture of $O_2/N_2$ (20:80 vol%) at 1 bar. These permeability and selectivity values surpassed the impressive results recently reported by Zhao et al., who prepared MMMs based on the combination of PIM-1 with magnetic responsive cobalt-based ionic liquid, and tested for $O_2/N_2$ separation obtaining $\alpha_{O_2/N_2}$ = ~5 with a $P_{O_2}$ of ~140 Barrer)[69].

Finally, for the $CO_2/CH_4$ gas pair the best improvement shown by an MMM over pristine polymer was obtained for PIM-TMN-Trip/MIL-101(Cr), with only a slight reduction of the ultra-permeability ($P_{CO_2}$ from 40000 to 32000 Barrer) (Fig. 10e), which is high compared to the recently reported value of 7000 Barrer by Huang et al.[70], combined with an increase in selectivity (from 7 to 9.5) for these difficult to separate gases. The $CO_2/CH_4$ selectivity

continued to increase after 2000 aging days, especially evident for a $CO_2/CH_4$ binary mixture (35:65 vol%), reaching a remarkable $\alpha CO_2/CH_4$=17, exceeded that obtained with the single gases and showing the size-sieving character of the MOF. The MMMs based on the dispersion of MIL-101(Cr) and MIL-177(Ti) into PIM-EA-TB exhibited an improvement of selectivity when compared to the neat PIM-EA-TB (from 8 to 11), which was retained after the aging period of ca. 2000 days (Fig. 10e-f)). In addition, for the binary mixture of $CO_2/CH_4$ (35:65 vol%) at 1 bar, the selectivity further increased up to $\alpha CO_2/CH_4$= 17 for both MMMs.

## 4 Conclusions

MMMs based on MIL-101(Cr) or MIL-177(Ti) using highly permeable PIM-EA-TB or PIM-TMN-Trip matrices were successfully obtained. SEM and EDX analysis of cross-sections of the MMMs confirmed good dispersions of the MOFs without evident defects or agglomeration. Following the typical MeOH treatment, all MMMs showed either increased selectivity, increased permeability, or both as compared to their pristine polymer counterparts. MIL-177(Ti) helped improve the selectivity for all gas pairs in both polymers, at the cost of a slight decrease in permeability for PIM-TMN-Trip. The selectivity of PIM-TMN-Trip was also increased by MIL-101(Cr), although accompanied by a slight decrease in permeability for gases of larger kinetic diameter. The combination of MIL-101(Cr) with PIM-EA-TB formed a MMM that enhanced both selectivity and permeability with values ranging from, $P_{H_2}$ from 6000 to 13000 Barrer with $\alpha_{H_2/CH_4}$ from 8 to 14; $P_{O_2}$ 1700 to 3000 Barrer and $\alpha_{O_2/N_2}$ from 4 to 5; $P_{CO_2}$ from 6000 to 10000 and $\alpha_{CO_2/CH_4}$ from 8 to 11, all approaching the 2015 upper bound. The comparison of experimental permeabilities with the predicted values by the Maxwell model for polymer PIM-EA-TB with MIL-101(Cr) and MIL-177(Ti) confirms the good dispersion and the absence of anomalies, whereas the deviation from the Maxwell model of the low $CO_2$ permeability for PIM-TMN-Trip with both MOFs suggests that the filler affects the bulk polymer properties, likely by occupying part of the polymer's free volume or due to increasing the rigidity of the matrix. The decrease in permeability due to aging, for the MMMs based on PIM-TMN-Trip/MIL-101(Cr) and MIL-177(Ti) is compensated by an increase in selectivity even by using gas mixtures. On the other hand, the MMMs based on PIM-EA-TB/MIL-101(Cr) showed good retention of the initially high permeability and selectivity upon aging, when compared to the neat polymer. Finally, for mixed gas analysis, the 2000 days aged PIM-EA-TB/MIL-101(Cr) showed greater selectivity for $CO_2/CH_4$ (from 10 to 25) and $CO_2/N_2$ (from 17 to 23) that than calculated from single gas permeabilities. The 2000 days aged PIM-

TMN-Trip/MIL-101(Cr) retained high $PCO_2$ of 15000 Barrer and moderate $\alpha CO_2/CH_4$ (from 12 to 17) and $\alpha CO_2/N_2$ selectivity (from 16 to 22), in both cases approaching the 2019 upper bound.

**Supplementary Materials**

**Acknowledgements**

The work leading to these results has received funding from the European Union's Seventh Framework Program (*FP7/2007-2013*) under *grant agreement* no. 608490, project $M^4CO_2$.

**References**

[1] Y. Wang, X. Ma, B.S. Ghanem, F. Alghunaimi, I. Pinnau, Y. Han, Polymers of intrinsic microporosity for energy-intensive membrane-based gas separations, Mater. Today Nano. 3 (2018) 69–95. https://doi.org/10.1016/J.MTNANO.2018.11.003.

[2] S. Kim, Y.M. Lee, Rigid and microporous polymers for gas separation membranes, Prog. Polym. Sci. 43 (2015) 1–32. https://doi.org/10.1016/j.progpolymsci.2014.10.005.

[3] M. Carta, Ladder Polymers of Intrinsic Microporosity (PIMs), in: Ladder Polym., Wiley, 2023: pp. 179–218. https://doi.org/10.1002/9783527833306.ch6.

[4] S. Bandehali, A. Ebadi Amooghin, H. Sanaeepur, R. Ahmadi, A. Fuoco, J.C. Jansen, S. Shirazian, Polymers of intrinsic microporosity and thermally rearranged polymer membranes for highly efficient gas separation, Sep. Purif. Technol. 278 (2022) 119513. https://doi.org/10.1016/j.seppur.2021.119513.

[5] N.B. McKeown, The structure-property relationships of Polymers of Intrinsic Microporosity (PIMs), Curr. Opin. Chem. Eng. 36 (2022) 100785. https://doi.org/10.1016/j.coche.2021.100785.

[6] B.D. Freeman, Basis of permeability/selectivity tradeoff relations in polymeric gas separation membranes, Macromolecules. 32 (1999) 375–380. https://doi.org/10.1021/ma9814548.

[7] P.M. Budd, B.S. Ghanem, S. Makhseed, N.B. McKeown, K.J. Msayib, C.E. Tattershall, Polymers of intrinsic microporosity (PIMs): robust, solution-processable, organic nanoporous materials, Chem. Commun. 4 (2004) 230–231.

https://doi.org/10.1039/b311764b.

[8] P.M. Budd, E.S. Elabas, B.S. Ghanem, S. Makhseed, N.B. McKeown, K.J. Msayib, C.E. Tattershall, D. Wang, Solution-Processed, Organophilic Membrane Derived from a Polymer of Intrinsic Microporosity, Adv. Mater. 16 (2004) 456–459. https://doi.org/10.1002/adma.200306053.

[9] L.M. Robeson, The upper bound revisited, J. Memb. Sci. 320 (2008) 390–400. https://doi.org/10.1016/j.memsci.2008.04.030.

[10] N.B. McKeown, The structure-property relationships of Polymers of Intrinsic Microporosity (PIMs), Curr. Opin. Chem. Eng. 36 (2022) 100785. https://doi.org/10.1016/j.coche.2021.100785.

[11] C.R. Mason, L. Maynard-Atem, K.W.J. Heard, B. Satilmis, P.M. Budd, K. Friess, M. Lanč, P. Bernardo, G. Clarizia, J.C. Jansen, Enhancement of CO2 Affinity in a Polymer of Intrinsic Microporosity by Amine Modification., Macromolecules. 47 (2014) 1021–1029. https://doi.org/10.1021/ma401869p.

[12] B. Satilmis, M. Lanč, A. Fuoco, C. Rizzuto, E. Tocci, P. Bernardo, G. Clarizia, E. Esposito, M. Monteleone, M. Dendisová, K. Friess, P.M. Budd, J.C. Jansen, Temperature and pressure dependence of gas permeation in amine-modified PIM-1, J. Memb. Sci. 555 (2018) 483–496. https://doi.org/10.1016/j.memsci.2018.03.039.

[13] C.R. Mason, L. Maynard-Atem, N.M. Al-Harbi, P.M. Budd, P. Bernardo, F. Bazzarelli, G. Clarizia, J.C. Jansen, Polymer of Intrinsic Microporosity Incorporating Thioamide Functionality: Preparation and Gas Transport Properties, Macromolecules. 44 (2011) 6471–6479. https://doi.org/10.1021/ma200918h.

[14] R. Swaidan, B.S. Ghanem, E. Litwiller, I. Pinnau, Pure- and mixed-gas CO2/CH4 separation properties of PIM-1 and an amidoxime-functionalized PIM-1, J. Memb. Sci. 457 (2014) 95–102. https://doi.org/10.1016/J.MEMSCI.2014.01.055.

[15] N. Du, H.B. Park, G.P. Robertson, M.M. Dal-Cin, T. Visser, L. Scoles, M.D. Guiver, Polymer nanosieve membranes for CO2-capture applications, Nat Mater. 10 (2011) 372–375.

[16] M. Carta, R. Malpass-Evans, M. Croad, Y. Rogan, J.C. Jansen, P. Bernardo, F. Bazzarelli, N.B. McKeown, An Efficient Polymer Molecular Sieve for Membrane Gas

Separations, Science (80-. ). 339 (2013) 303–307. https://doi.org/10.1126/science.1228032.

[17] I. Rose, C.G. Bezzu, M. Carta, B. Comesanã-Gándara, E. Lasseuguette, M.C. Ferrari, P. Bernardo, G. Clarizia, A. Fuoco, J.C. Jansen, K.E. Hart, T.P. Liyana-Arachchi, C.M. Colina, N.B. McKeown, Polymer ultrapermeability from the inefficient packing of 2D chains, Nat. Mater. 16 (2017) 932–937. https://doi.org/10.1038/nmat4939.

[18] I. Rose, M. Carta, R. Malpass-Evans, M.-C. Ferrari, P. Bernardo, G. Clarizia, J.C. Jansen, N.B. McKeown, Highly Permeable Benzotriptycene-Based Polymer of Intrinsic Microporosity, ACS Macro Lett. 4 (2015) 912–915. https://doi.org/10.1021/acsmacrolett.5b00439.

[19] M. Carta, M. Croad, R. Malpass-Evans, J.C. Jansen, P. Bernardo, G. Clarizia, K. Friess, M. Lanč, N.B. McKeown, Triptycene Induced Enhancement of Membrane Gas Selectivity for Microporous Tröger's Base Polymers, Adv. Mater. 26 (2014) 3526–3531. https://doi.org/10.1002/adma.201305783.

[20] A. Fuoco, B. Comesaña-Gándara, M. Longo, E. Esposito, M. Monteleone, I. Rose, C.G. Bezzu, M. Carta, N.B. McKeown, J.C. Jansen, Temperature Dependence of Gas Permeation and Diffusion in Triptycene-Based Ultrapermeable Polymers of Intrinsic Microporosity, ACS Appl. Mater. Interfaces. 10 (2018) 36475–36482. https://doi.org/10.1021/acsami.8b13634.

[21] B. Comesaña-Gándara, J. Chen, C.G. Bezzu, M. Carta, I. Rose, M.-C. Ferrari, E. Esposito, A. Fuoco, J.C. Jansen, N.B. McKeown, Redefining the Robeson upper bounds for CO 2 /CH 4 and CO 2 /N 2 separations using a series of ultrapermeable benzotriptycene-based polymers of intrinsic microporosity, Energy Environ. Sci. 12 (2019) 2733–2740. https://doi.org/10.1039/C9EE01384A.

[22] J. Chen, M. Longo, A. Fuoco, E. Esposito, M. Monteleone, B. Comesaña Gándara, J. Carolus Jansen, N.B. McKeown, Dibenzomethanopentacene-Based Polymers of Intrinsic Microporosity for Use in Gas-Separation Membranes, Angew. Chemie - Int. Ed. 62 (2023) 1–9. https://doi.org/10.1002/anie.202215250.

[23] K. Chen, L. Ni, H. Zhang, C. Xiao, L. Li, X. Guo, J. Qi, C. Wang, X. Sun, J. Li, Incorporating KAUST-7 into PIM-1 towards mixed matrix membranes with long-term stable CO2/CH4 separation performance, J. Memb. Sci. 661 (2022).

https://doi.org/10.1016/j.memsci.2022.120848.

[24] C.H. Lau, P.T. Nguyen, M.R. Hill, A.W. Thornton, K. Konstas, C.M. Doherty, R.J. Mulder, L. Bourgeois, A.C.Y. Liu, D.J. Sprouster, J.P. Sullivan, T.J. Bastow, A.J. Hill, D.L. Gin, R.D. Noble, Ending aging in super glassy polymer membranes, Angew. Chemie - Int. Ed. 53 (2014) 5322–5326. https://doi.org/10.1002/anie.201402234.

[25] M. Carta, A.R. Antonangelo, J.C. Jansen, M. Longo, The Difference in Performance and Compatibility between Crystalline and Amorphous Fillers in Mixed Matrix Membranes for Gas Separation (MMMs), Polymers (Basel). 15 (2023) 2951. https://doi.org/10.3390/polym15132951.

[26] G. Dai, Q. Zhang, S. Xiong, L. Deng, Z. Gao, A. Chen, X. Li, C. Pan, J. Tang, G. Yu, Building interfacial compatible PIM-1-based mixed-matrix membranes with β-ketoenamine-linked COF fillers for effective CO2/N2 separation, J. Memb. Sci. 676 (2023) 121561. https://doi.org/10.1016/j.memsci.2023.121561.

[27] B. Seoane, J. Coronas, I. Gascon, M.E. Benavides, O. Karvan, J. Caro, F. Kapteijn, J. Gascon, Metal-organic framework based mixed matrix membranes: A solution for highly efficient CO2 capture?, Chem. Soc. Rev. 44 (2015) 2421–2454. https://doi.org/10.1039/c4cs00437j.

[28] W. Chen, Z. Zhang, C. Yang, J. Liu, H. Shen, K. Yang, Z. Wang, PIM-based mixed-matrix membranes containing MOF-801/ionic liquid nanocomposites for enhanced CO2 separation performance, J. Memb. Sci. 636 (2021) 119581. https://doi.org/10.1016/j.memsci.2021.119581.

[29] N. Tien-Binh, D. Rodrigue, S. Kaliaguine, In-situ cross interface linking of PIM-1 polymer and UiO-66-NH2 for outstanding gas separation and physical aging control, J. Memb. Sci. 548 (2018) 429–438. https://doi.org/10.1016/J.MEMSCI.2017.11.054.

[30] Y. Sun, C. Geng, Z. Zhang, Z. Qiao, C. Zhong, Two-dimensional basic cobalt carbonate supported ZIF-67 composites towards mixed matrix membranes for efficient CO2/N2 separation, J. Memb. Sci. 661 (2022) 120928. https://doi.org/10.1016/j.memsci.2022.120928.

[31] F. Begni, E. Lasseuguette, G. Paul, C. Bisio, L. Marchese, G. Gatti, M.C. Ferrari, Hyper-Cross-Linked Polymers with Sulfur-Based Functionalities for the Prevention of Aging

Effects in PIM-1 Mixed Matrix Membranes, ACS Appl. Polym. Mater. (2023). https://doi.org/10.1021/acsapm.3c00246.

[32] L. Hao, K.S. Liao, T.S. Chung, Photo-oxidative PIM-1 based mixed matrix membranes with superior gas separation performance, J. Mater. Chem. A. (2015). https://doi.org/10.1039/c5ta03776j.

[33] A.F. Bushell, M.P. Attfield, C.R. Mason, P.M. Budd, Y. Yampolskii, L. Starannikova, A. Rebrov, F. Bazzarelli, P. Bernardo, J. Carolus Jansen, M. Lanč, K. Friess, V. Shantarovich, V. Gustov, V. Isaeva, Gas permeation parameters of mixed matrix membranes based on the polymer of intrinsic microporosity PIM-1 and the zeolitic imidazolate framework ZIF-8, J. Memb. Sci. 427 (2013) 48–62. https://doi.org/10.1016/j.memsci.2012.09.035.

[34] Q. Zhao, K. Niu, R. Wang, S. Lian, R. Li, G. Zang, C. Song, Pre-anchoring matrix onto zeolitic imidazolate frameworks towards defect-free mixed matrix membranes for efficient CO2 separation, J. Memb. Sci. 683 (2023) 121869. https://doi.org/10.1016/j.memsci.2023.121869.

[35] Z. Chen, X. Meng, Y. Fan, N. Li, L. Wu, S. Luo, W. Xie, C. Wang, Two morphology distinct fillers with chemical similarity incorporated into Tröger' base polymers towards enhanced gas separation, J. Memb. Sci. 685 (2023) 121964. https://doi.org/10.1016/j.memsci.2023.121964.

[36] a. Y. Alentiev, G.N. Bondarenko, Y. V. Kostina, V.P. Shantarovich, S.N. Klyamkin, V.P. Fedin, K. a. Kovalenko, Y.P. Yampolskii, PIM-1/MIL-101 hybrid composite membrane material: Transport properties and free volume, Pet. Chem. 54 (2014) 477–481. https://doi.org/10.1134/S0965544114070020.

[37] M. Khdhayyer, A.F. Bushell, P.M. Budd, M.P. Attfield, D. Jiang, A.D. Burrows, E. Esposito, P. Bernardo, M. Monteleone, A. Fuoco, G. Clarizia, F. Bazzarelli, A. Gordano, J.C. Jansen, Mixed matrix membranes based on MIL-101 metal–organic frameworks in polymer of intrinsic microporosity PIM-1, Sep. Purif. Technol. 212 (2019) 545–554. https://doi.org/10.1016/j.seppur.2018.11.055.

[38] J. Ma, Y. Ying, X. Guo, H. Huang, D. Liu, C. Zhong, Fabrication of mixed-matrix membrane containing metal-organic framework composite with task-specific ionic liquid for efficient CO2 separation, J. Mater. Chem. A. 4 (2016) 7281–7288.

https://doi.org/10.1039/c6ta02611g.

[39] Z. Wang, H. Ren, S. Zhang, F. Zhang, J. Jin, Polymers of intrinsic microporosity/metal–organic framework hybrid membranes with improved interfacial interaction for high-performance CO2 separation, J. Mater. Chem. A. 5 (2017) 10968–10977. https://doi.org/10.1039/C7TA01773A.

[40] M.R. Khdhayyer, E. Esposito, A. Fuoco, M. Monteleone, L. Giorno, J.C. Jansen, M.P. Attfield, P.M. Budd, Mixed matrix membranes based on UiO-66 MOFs in the polymer of intrinsic microporosity PIM-1, Sep. Purif. Technol. 173 (2017) 304–313. https://doi.org/10.1016/j.seppur.2016.09.036.

[41] D.Y. Kang, J.S. Lee, Challenges in Developing MOF-Based Membranes for Gas Separation, Langmuir. 39 (2023) 2871–2880. https://doi.org/10.1021/acs.langmuir.2c03458.

[42] B. Ghalei, K. Sakurai, Y. Kinoshita, K. Wakimoto, A.P. Isfahani, Q. Song, K. Doitomi, S. Furukawa, H. Hirao, H. Kusuda, S. Kitagawa, E. Sivaniah, Enhanced selectivity in mixed matrix membranes for CO2 capture through efficient dispersion of amine-functionalized MOF nanoparticles, Nat. Energy. (2017). https://doi.org/10.1038/nenergy.2017.86.

[43] G. Férey, C. Mellot-Draznieks, C. Serre, F. Millange, J. Dutour, S. Surblé, I. Margiolaki, A Chromium Terephtalate-Based Solid with Unusually Large Pore Volumes and Surface Area, Science (80-. ). 309 (2005) 2040. https://doi.org/10.1126/science.1116275.

[44] S. Wang, T. Kitao, N. Guillou, M. Wahiduzzaman, C. Martineau-Corcos, F. Nouar, A. Tissot, L. Binet, N. Ramsahye, S. Devautour-Vinot, S. Kitagawa, S. Seki, Y. Tsutsui, V. Briois, N. Steunou, G. Maurin, T. Uemura, C. Serre, A phase transformable ultrastable titanium-carboxylate framework for photoconduction, Nat. Commun. 9 (2018) 1–9. https://doi.org/10.1038/s41467-018-04034-w.

[45] J.W. Yoon, H. Chang, S.J. Lee, Y.K. Hwang, D.Y. Hong, S.K. Lee, J.S. Lee, S. Jang, T.U. Yoon, K. Kwac, Y. Jung, R.S. Pillai, F. Faucher, A. Vimont, M. Daturi, G. Férey, C. Serre, G. Maurin, Y.S. Bae, J.S. Chang, Selective nitrogen capture by porous hybrid materials containing accessible transition metal ion sites, Nat. Mater. (2017). https://doi.org/10.1038/nmat4825.

[46] A. Demessence, P. Horcajada, C. Serre, C. Boissière, D. Grosso, C. Sanchez, G. Férey, Elaboration and properties of hierarchically structured optical thin films of MIL-101(Cr), Chem. Commun. (2009). https://doi.org/10.1039/b915011k.

[47] P. Bernardo, V. Scorzafave, G. Clarizia, E. Tocci, J.C. Jansen, A. Borgogno, R. Malpass-Evans, N.B. McKeown, M. Carta, F. Tasselli, Thin film composite membranes based on a polymer of intrinsic microporosity derived from Tröger's base: A combined experimental and computational investigation of the role of residual casting solvent, J. Memb. Sci. 569 (2019) 17–31. https://doi.org/10.1016/J.MEMSCI.2018.10.001.

[48] J.C. Jansen, K. Friess, E. Drioli, Organic vapour transport in glassy perfluoropolymer membranes: A simple semi-quantitative approach to analyze clustering phenomena by time lag measurements, J. Memb. Sci. 367 (2011) 141–151. https://doi.org/10.1016/j.memsci.2010.10.063.

[49] J. Crank, The mathematics of diffusion, 2nd ed., Clarendon Press, n.d.

[50] S.C. Fraga, M. Monteleone, M. Lanč, E. Esposito, A. Fuoco, L. Giorno, K. Pilnáček, K. Friess, M. Carta, N.B. McKeown, P. Izák, Z. Petrusová, J.G. Crespo, C. Brazinha, J.C. Jansen, A novel time lag method for the analysis of mixed gas diffusion in polymeric membranes by on-line mass spectrometry: Method development and validation, J. Memb. Sci. 561 (2018) 39–58. https://doi.org/10.1016/j.memsci.2018.04.029.

[51] M. Gui, V. Wee, A. Chinnappan, S. Ramakrishna, Elucidating Improvements to MIL-101 ( Cr )' s Porosity and Particle Size Distributions based on Innovations and Fine-Tuning in Synthesis Procedures, 101 (2023). https://doi.org/10.1002/admi.202300065.

[52] P.L. Llewellyn, S. Bourrelly, C. Serre, A. Vimont, M. Daturi, L. Hamon, G. De Weireld, J.-S. Chang, D.-Y. Hong, Y. Kyu Hwang, S. Hwa Jhung, G. Férey, High Uptakes of CO 2 and CH 4 in Mesoporous Metal□Organic Frameworks MIL-100 and MIL-101, Langmuir. 24 (2008) 7245–7250. https://doi.org/10.1021/la800227x.

[53] Z. Li, J.P. Lowe, P.J. Fletcher, M. Carta, N.B. McKeown, F. Marken, Tuning and Coupling Irreversible Electroosmotic Water Flow in Ionic Diodes: Methylation of an Intrinsically Microporous Polyamine (PIM-EA-TB), ACS Appl. Mater. Interfaces. 15 (2023) 42369–42377. https://doi.org/10.1021/acsami.3c10220.

[54] A.R. Antonangelo, N. Hawkins, E. Tocci, C. Muzzi, A. Fuoco, M. Carta, Tröger's Base

Network Polymers of Intrinsic Microporosity (TB-PIMs) with Tunable Pore Size for Heterogeneous Catalysis, J. Am. Chem. Soc. 144 (2022) 15581–15594. https://doi.org/10.1021/jacs.2c04739.

[55] F. Marken, E. Madrid, Y. Zhao, M. Carta, N.B. McKeown, Polymers of Intrinsic Microporosity in Triphasic Electrochemistry: Perspectives, ChemElectroChem. 6 (2019) 4332–4342. https://doi.org/10.1002/celc.201900717.

[56] R. Malpass-Evans, I. Rose, A. Fuoco, P. Bernardo, G. Clarizia, N.B. McKeown, J.C. Jansen, M. Carta, Effect of bridgehead methyl substituents on the gas permeability of tröger's-base derived polymers of intrinsic microporosity, Membranes (Basel). 10 (2020). https://doi.org/10.3390/membranes10040062.

[57] S.A. Felemban, C.G. Bezzu, B. Comesaña-Gándara, J.C. Jansen, A. Fuoco, E. Esposito, M. Carta, N.B. McKeown, Synthesis and gas permeation properties of tetraoxidethianthrene-based polymers of intrinsic microporosity, J. Mater. Chem. A. 9 (2021) 2840–2849. https://doi.org/10.1039/D0TA10134F.

[58] R. Mahajan, W.J. Koros, Factors Controlling Successful Formation of Mixed-Matrix Gas Separation Materials, Ndustrial Eng. Chem. Res. 39 (2000) 2692–2696. https://doi.org/10.1021/ie990799r.

[59] S.A. Hashemifard, A.F. Ismail, T. Matsuura, A new theoretical gas permeability model using resistance modeling for mixed matrix membrane systems, J. Memb. Sci. 350 (2010) 259–268. https://doi.org/10.1016/j.memsci.2009.12.036.

[60] B. Shimekit, H. Mukhtar, T. Murugesan, Prediction of the relative permeability of gases in mixed matrix membranes, J. Memb. Sci. 373 (2011) 152–159. https://doi.org/10.1016/j.memsci.2011.02.038.

[61] T.-S. Chung, L.Y. Jiang, Y. Li, S. Kulprathipanja, Mixed matrix membranes (MMMs) comprising organic polymers with dispersed inorganic fillers for gas separation, Prog. Polym. Sci. 32 (2007) 483–507. https://doi.org/10.1016/j.progpolymsci.2007.01.008.

[62] S. Keskin, D.S. Sholl, Selecting metal organic frameworks as enabling materials in mixed matrix membranes for high efficiency natural gas purification, Energy Environ. Sci. 3 (2010) 343–351. https://doi.org/10.1039/B923980B.

[63] S.A. Hashemifard, A.F. Ismail, T. Matsuura, Prediction of gas permeability in mixed

matrix membranes using theoretical models, J. Memb. Sci. 347 (2010) 53–61. https://doi.org/10.1016/j.memsci.2009.10.005.

[64] J.C. Maxwell, A Treatise on Electricity and Magnetism Volume 1, Cambridge University Press, 2010.

[65] F.N. Al-Rowaili, M. Khaled, A. Jamal, U. Zahid, Mixed matrix membranes for H2/CO2 gas separation- a critical review, Fuel. 333 (2023) 126285. https://doi.org/10.1016/j.fuel.2022.126285.

[66] L.M. Robeson, Correlation of separation factor versus permeability for polymeric membranes, J. Memb. Sci. 62 (1991) 165–185. https://doi.org/10.1016/0376-7388(91)80060-J.

[67] R. Swaidan, B. Ghanem, I. Pinnau, Fine-Tuned Intrinsically Ultramicroporous Polymers Redefine the Permeability/Selectivity Upper Bounds of Membrane-Based Air and Hydrogen Separations, ACS Macro Lett. 4 (2015) 947–951. https://doi.org/10.1021/acsmacrolett.5b00512.

[68] R. Hou, B.S. Ghanem, S.J.D. Smith, C.M. Doherty, C. Setter, H. Wang, I. Pinnau, M.R. Hill, Highly permeable and selective mixed-matrix membranes for hydrogen separation containing PAF-1, J. Mater. Chem. A. 8 (2020) 14713–14720. https://doi.org/10.1039/d0ta05071g.

[69] H. Zhao, T. Song, X. Ding, R. Cai, X. Tan, Y. Zhang, PIM-1 mixed matrix membranes incorporated with magnetic responsive cobalt-based ionic liquid for O2/N2 separation, J. Memb. Sci. 679 (2023) 1–7. https://doi.org/10.1016/j.memsci.2023.121713.

[70] X. Huang, L. Chen, S. Chen, P. Su, W. Li, Reconstruction of mixed matrix membranes by in situ vapor aminolysis for CO2/N2 and CH4/N2 separations, J. Memb. Sci. 685 (2023) 121984. https://doi.org/10.1016/j.memsci.2023.121984.

[71] T.T. Moore, W.J. Koros, Non-ideal effects in organic-inorganic materials for gas separation membranes, J. Mol. Struct. 739 (2005) 87–98. https://doi.org/10.1016/j.molstruc.2004.05.043.

**Supplementary Information**

# Mixed matrix membranes based on MIL-101(Cr) and MIL-177(Ti) metal–organic frameworks in Polymers of Intrinsic Microporosity

## Maxwell model

The Maxwell model is usually employed to describe the gas transport in mixed matrix membranes [58–61]:

$$P_{MMM} = P_c\left|\frac{P_d + 2P_c - 2\Phi_d(P_c - P_d)}{P_d + 2P_c + \Phi_d(P_c - P_d)}\right| \quad \text{(Eq. 2)}$$

where the $P_{MMM}$ is the effective permeability of the mixed matrix membrane, $P_c$ and $P_d$ represent the gas permeabilities in the continuous and dispersed phase, respectively and $\Phi_d$ is the volume fraction of dispersed phase. The gas transport in an MMM can occur in different ways and several, fundamentally different, cases may occur at the same time, as it was described in detail by Koros et. al. [71].

*Case 0*

Generally, the permeability of the gases through the dispersed phase lies between the two extreme cases discussed above, and $0 \ll Pd \ll \infty$. The fillers exhibit an intrinsic finite permeability and, as a result, the MMM will have an effective permeability, different from that of the polymer matrix. This requires that the MOFs particles are well distributed within the polymer matrix and they adhere to the polymer without blocking the pores.

*Case I*

In this situation, the permeability of the gas in the dispersed phase is much lower than that of the continuous phase: $P_d \ll P_c$. This can happen for two different reasons, when occurs a partial blockage of the MOF by the polymer phase or when the fillers behave as impermeable obstacles and they can affect the total free volume of the polymer matrix, typically decreasing its permeability.

*Case II*

In this case, the permeability of the gas in the dispersed phase, and around the particles, is much higher than that of the continuous phase: $P_d \gg P_c$. This occurs when the interaction between the

polymer and filler particles is poor. The polymer chains do not completely adhere to the surface of the fillers giving rise to the formation of undesirable channels between both phases. At low filler loadings, this result in a higher permeability but constant selectivity, also described by Koros as case II. At relatively high filler loadings, continuous channels are formed across the membrane, which also deteriorates the selectivity of the MMM, this is described by Koros as case III [71].

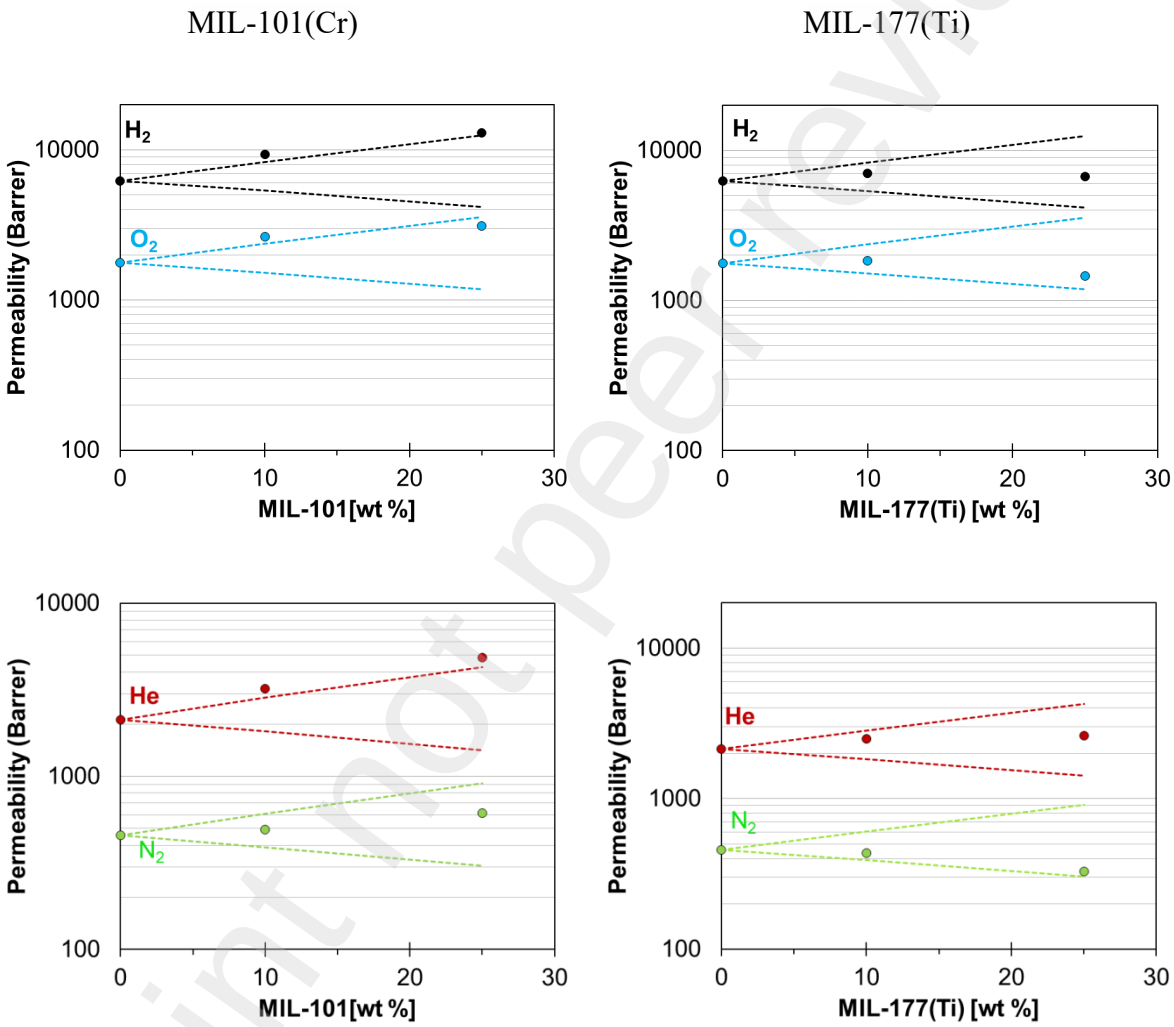

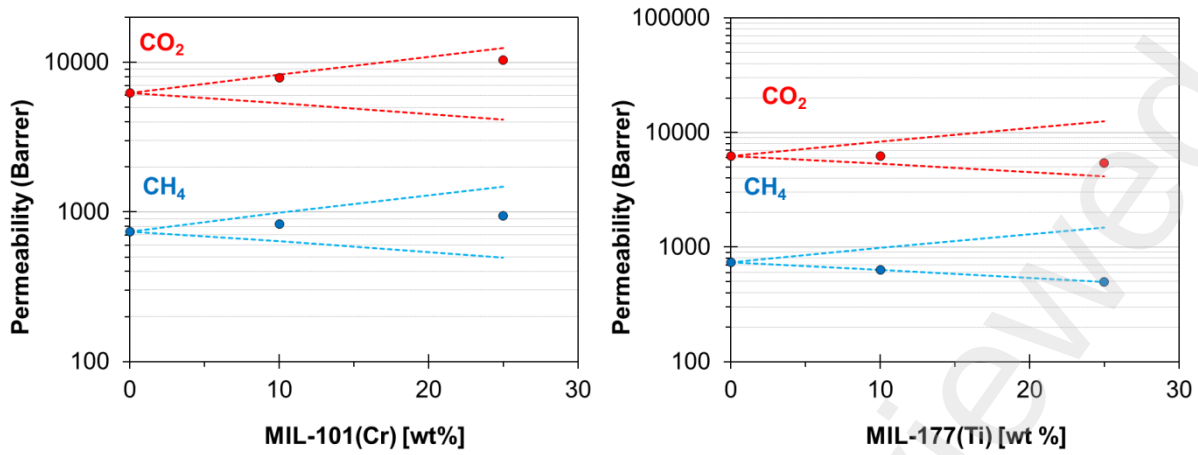


**Fig.S 1** The $H_2$, $N_2$, He, $N_2$, $CO_2$ and $CH_4$ permeabilities as a function of the MOFs concentration for MIL-101(Cr) (on the left) and MIL-177(Ti) (on the right) loaded into the PIM-EA-TB after methanol treatment. The lines correspond to the fit of the experimental data with Maxwell equation for the lower limit and the upper limit with Pd = 0 and Pd = 1, respectively

MIL-101(Cr) MIL-177(Ti)

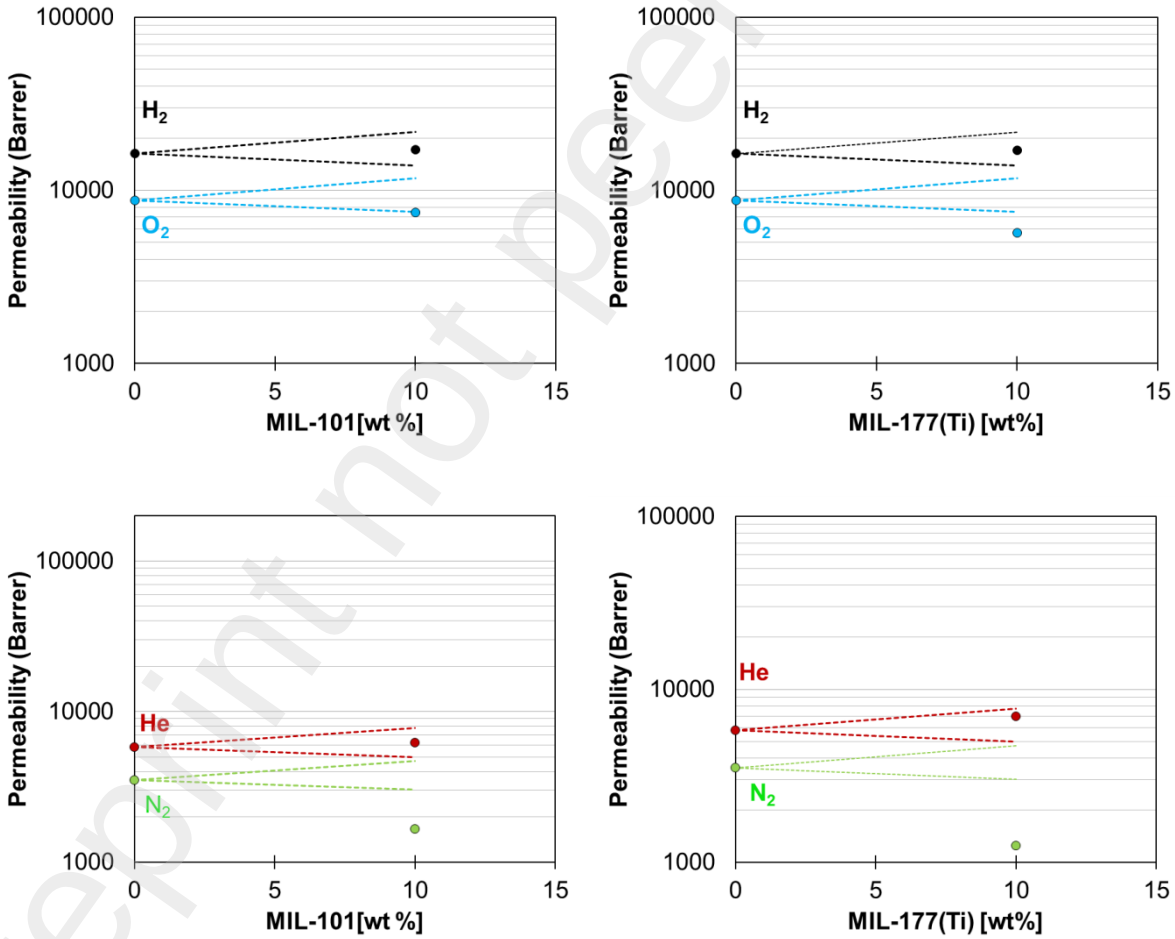

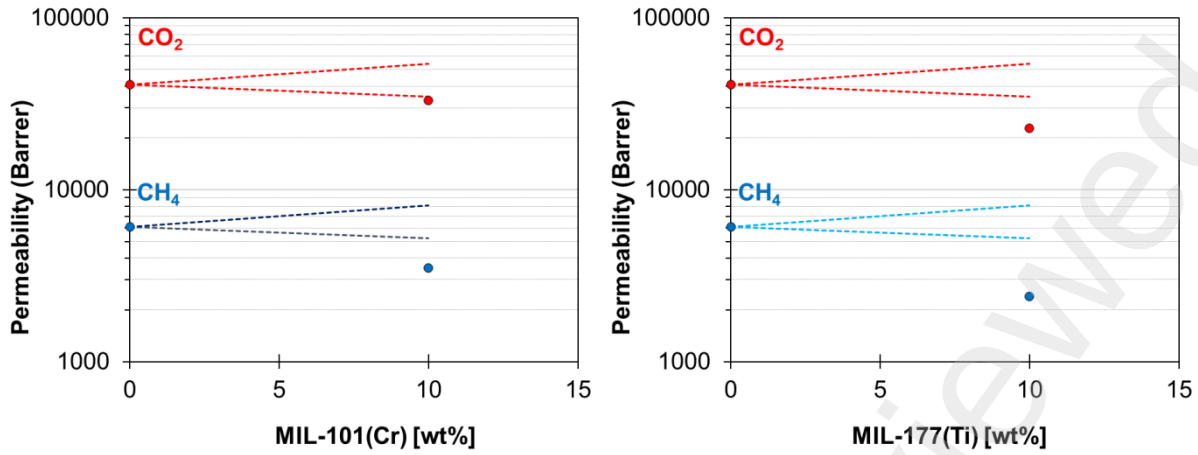


**Fig.S 2** The $H_2$, $N_2$, He, $N_2$, $CO_2$ and $CH_4$ permeabilities as a function of the MOFs concentration for MIL-101(Cr) (on the left) and MIL-177(Ti) (on the right) loaded into the PIM-TMN-Trip after methanol treatment. The lines correspond to the fit of the experimental data with Maxwell equation for the lower limit and the upper limit with Pd = 0 and Pd = 1, respectively.

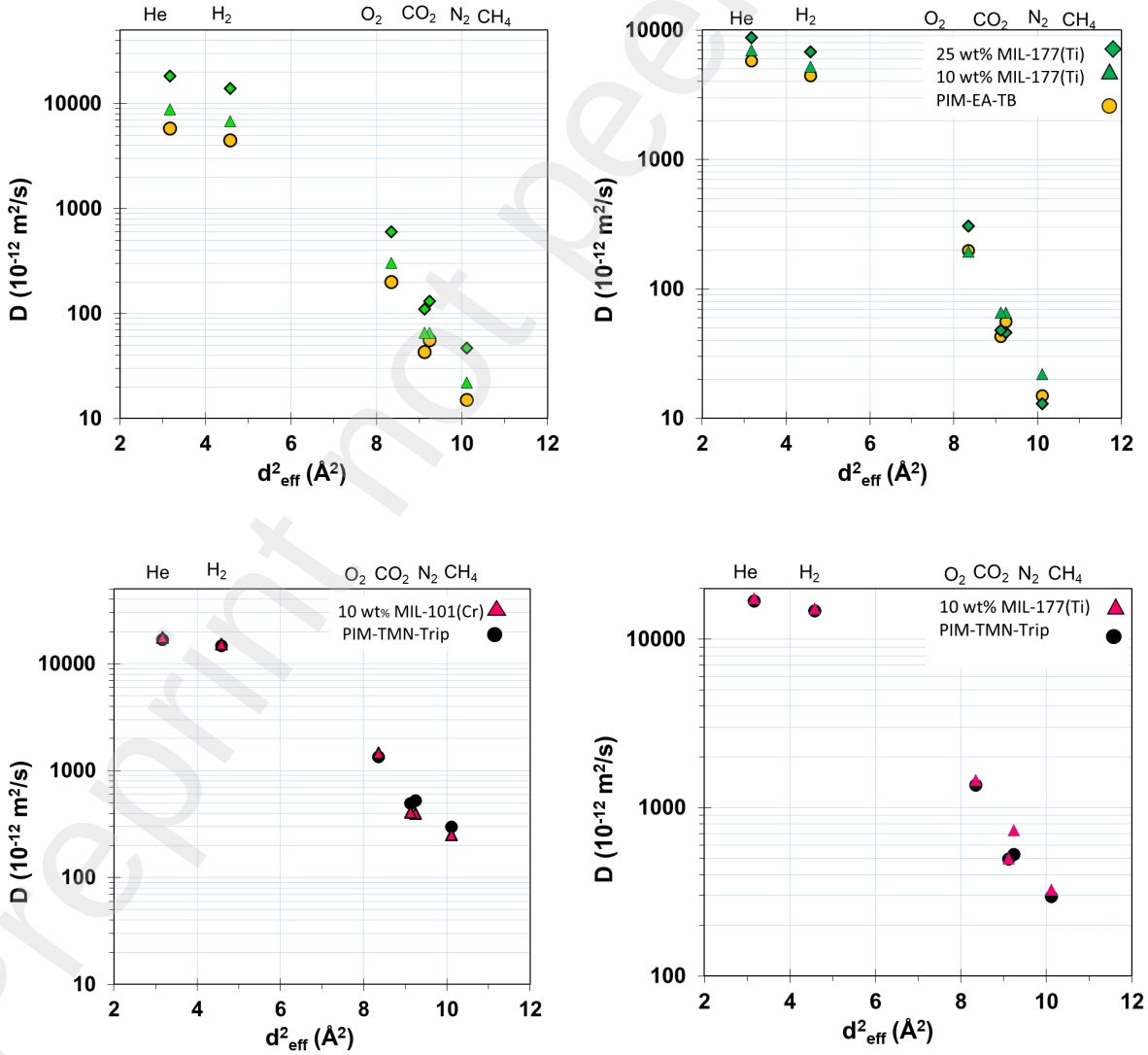

**Fig.S 3** Correlation of the diffusion coefficient with the square of the Teplyakov-Meares gas diameter for MMMs based on PIM-EA($Me_2$)-TB and PIM-TMN-Trip and their respective neat polymers.

**Table S-1 P**ermeability, diffusion and solubility coefficients, and respective selectivity of neat PIM-EA($Me_2$)-TB and PIM-EA($Me_2$)-TB/MIL-101 for MeOH, thermal and aging conditioning of membranes.

| **PIM-EA-TB/MIL-101(Cr)_MeOH** | | | | | | | | | | | |
|---|---|---|---|---|---|---|---|---|---|---|---|
| **MIL-101(Cr)** | Permeability [Barrer] | | | | | | α ($P_A/P_B$) | | | | |
| [wt%] | $N_2$ | $O_2$ | $CO_2$ | $CH_4$ | $H_2$ | He | $CO_2/N_2$ | $CO_2/CH_4$ | $H_2/CH_4$ | $H_2/N_2$ | $O_2/N_2$ |
| 0 | 455 | 1776 | 6231 | 741 | 6232 | 2128 | 13.7 | 8.41 | 8.41 | 13.7 | 3.91 |
| 10 | 494 | 2636 | 7908 | 830 | 9346 | 3216 | 16.0 | 9.5 | 11.3 | 18.9 | 5.34 |
| 25 | 615 | 3126 | 10313 | 944 | 13041 | 4845 | 16.8 | 10.9 | 13.8 | 21.2 | 5.08 |
| **MIL-101(Cr)** | Dx [10-12 $m^2s^{-1}$] | | | | | | α ($D_A/D_B$) | | | | |
| [wt%] | $N_2$ | $O_2$ | $CO_2$ | $CH_4$ | $H_2$ | He | $CO_2/N_2$ | $CO_2/CH_4$ | $H_2/CH_4$ | $H_2/N_2$ | $O_2/N_2$ |
| 0 | 56 | 199 | 43 | 15 | 4459 | 5780 | 0.77 | 2.86 | 299 | 80 | 3.59 |
| 10 | 66 | 305 | 66 | 22 | 6804 | 8783 | 1.00 | 3.02 | 313 | 104 | 4.66 |
| 25 | 131 | 599 | 111 | 47 | 13967 | 18341 | 0.85 | 2.34 | 294 | 106 | 4.56 |
| **MIL-101(Cr)** | Sx [$cm^3$(STP) $cm^{-3}$ $bar^{-1}$] | | | | | | α ($S_A/S_B$) | | | | |
| [wt%] | $N_2$ | $O_2$ | $CO_2$ | $CH_4$ | $H_2$ | He | $CO_2/N_2$ | $CO_2/CH_4$ | $H_2/CH_4$ | $H_2/N_2$ | $O_2/N_2$ |
| 0 | 6.14 | 6.69 | 110 | 37.3 | 1.05 | 0.28 | 17.9 | 2.94 | 0.03 | 0.17 | 1.09 |
| 10 | 4.28 | 4.61 | 76.7 | 22.8 | 0.69 | 0.17 | 18.0 | 3.37 | 0.03 | 0.16 | 1.08 |
| 25 | 3.51 | 3.92 | 69.6 | 14.9 | 0.70 | 0.20 | 19.8 | 4.67 | 0.05 | 0.20 | 1.11 |
| **PIM-EA-TB/ MIL-101(Cr)_T°C** | | | | | | | | | | | |
| **MIL-101(Cr)** | Permeability [Barrer] | | | | | | α ($P_A/P_B$) | | | | |
| [wt%] | $N_2$ | $O_2$ | $CO_2$ | $CH_4$ | $H_2$ | He | $CO_2/N_2$ | $CO_2/CH_4$ | $H_2/CH_4$ | $H_2/N_2$ | $O_2/N_2$ |
| 0 | 375 | 1636 | 5125 | 622 | 5500 | 1940 | 13.7 | 8.2 | 8.8 | 14.658 | 4.4 |
| 10 | 510 | 2277 | 7495 | 775 | 7979 | 2794 | 14.7 | 9.7 | 10.3 | 15.62 | 4.5 |
| 25 | 610 | 2891 | 9238 | 911 | 11176 | 4139 | 15.2 | 10.1 | 12.3 | 18.3 | 4.7 |
| **MIL-101** | Dx [10-12 $m^2s^{-1}$] | | | | | | α ($D_A/D_B$) | | | | |
| [wt%] | $N_2$ | $O_2$ | $CO_2$ | $CH_4$ | $H_2$ | He | $CO_2/N_2$ | $CO_2/CH_4$ | $H_2/CH_4$ | $H_2/N_2$ | $O_2/N_2$ |
| 0 | 36 | 160 | 36 | 14 | 4260 | 4899 | 1.00 | 2.54 | 297.8 | 117.9 | 4.43 |
| 10 | 25 | 128 | 30 | 8 | 3270 | 4678 | 1.22 | 3.95 | 425.8 | 131.1 | 5.12 |
| 25 | 117 | 525 | 121 | 41 | 12992 | 15981 | 1.04 | 2.93 | 314.8 | 111.2 | 4.50 |
| **MIL-101(Cr)** | Sx [$cm^3$(STP) $cm^{-3}$ $bar^{-1}$] | | | | | | α ($S_A/S_B$) | | | | |
| [wt%] | $N_2$ | $O_2$ | $CO_2$ | $CH_4$ | $H_2$ | He | $CO_2/N_2$ | $CO_2/CH_4$ | $H_2/CH_4$ | $H_2/N_2$ | $O_2/N_2$ |
| 0 | 7.8 | 7.7 | 105.8 | 32.6 | 1.0 | 0.3 | 13.6 | 3.24 | 0.03 | 0.12 | 0.98 |
| 10 | 6.0 | 5.6 | 84.6 | 27.2 | 0.9 | 0.2 | 14.1 | 3.11 | 0.03 | 0.16 | 0.94 |
| 25 | 3.9 | 4.1 | 57.3 | 16.6 | 0.6 | 0.2 | 14.6 | 3.46 | 0.04 | 0.16 | 1.05 |
| **PIM-EA-TB/ MIL-101(Cr)_Aged** | | | | | | | | | | | |
| **MIL-101(Cr)** | Permeability [Barrer] | | | | | | α ($P_A/P_B$) | | | | |
| [wt%] | $N_2$ | $O_2$ | $CO_2$ | $CH_4$ | $H_2$ | He | $CO_2/N_2$ | $CO_2/CH_4$ | $H_2/CH_4$ | $H_2/N_2$ | $O_2/N_2$ |
| 0 (860d) | 94 | 375 | 1511 | 139 | 1225 | 478 | 16.1 | 10.9 | 8.8 | 13 | 4.0 |
| 25 (30d) | 431 | 1820 | 5891 | 535 | 8109 | 3192 | 13.7 | 11.0 | 15.2 | 19 | 4.2 |
| 25(2000d) | 200 | 965 | 3463 | 323 | 4650 | 1746 | 17.35 | 10.73 | 14.4 | 23.30 | 4.84 |

| **MIL-101(Cr)** | | | Dx [10-12 $m^2s^{-1}$] | | | | | α ($D_A/D_B$) | | | |
|---|---|---|---|---|---|---|---|---|---|---|---|
| [wt%] | $N_2$ | $O_2$ | $CO_2$ | $CH_4$ | $H_2$ | He | $CO_2/N_2$ | $CO_2/CH_4$ | $H_2/CH_4$ | $H_2/N_2$ | $O_2/N_2$ |
| 0 | 20 | 73 | 21 | 6 | 1885 | 2777 | 1.06 | 3.34 | 298 | 94.5 | 3.67 |
| 25 (30d) | 82 | 311 | 70 | 25 | 7941 | 10303 | 0.85 | 2.80 | 319 | 97.2 | 3.80 |
| **MIL-101(Cr)** | | | Sx [$cm^3$(STP) $cm^{-3}$ $bar^{-1}$] | | | | | α ($S_A/S_B$) | | | |
| [wt%] | $N_2$ | $O_2$ | $CO_2$ | $CH_4$ | $H_2$ | He | $CO_2/N_2$ | $CO_2/CH_4$ | $H_2/CH_4$ | $H_2/N_2$ | $O_2/N_2$ |
| 0 | 3.54 | 3.84 | 53.81 | 16.46 | 0.49 | 0.13 | 15.2 | 3.27 | 0.03 | 0.14 | 1.08 |
| 25 (30d) | 3.95 | 4.39 | 63.30 | 16.11 | 0.77 | 0.23 | 16.0 | 3.93 | 0.05 | 0.19 | 1.11 |

**Table S-2** Pure gas permeability, solubility and diffusion coefficients, and respective selectivity of neat PIM-EA($Me_2$)-TB and PIM-EA($Me_2$)-TB/MIL-177(Ti) for MeOH, thermal and aging conditioning of membranes.

| **PIM-EA-TB/ MIL-177(Ti)_MeOH** | | | | | | | | | | | |
|---|---|---|---|---|---|---|---|---|---|---|---|
| **MIL-177(Ti)** | | | Permeability [Barrer] | | | | | α ($P_A/P_B$) | | | |
| [wt%] | $N_2$ | $O_2$ | $CO_2$ | $CH_4$ | $H_2$ | He | $CO_2/N_2$ | $CO_2/CH_4$ | $H_2/CH_4$ | $H_2/N_2$ | $O_2/N_2$ |
| 0 | 455 | 1776 | 6231 | 741 | 6232 | 2128 | 13.7 | 8.41 | 8.41 | 13.7 | 3.91 |
| 10 | 436 | 1837 | 6198 | 633 | 7001 | 2492 | 14.2 | 9.80 | 11.1 | 16.1 | 4.21 |
| 25 | 329 | 1451 | 5389 | 496 | 6674 | 2632 | 16.4 | 10.9 | 13.5 | 20.2 | 4.4 |
| **MIL-177(Ti)** | | | Dx [10-12 $m^2s^{-1}$] | | | | | α ($D_A/D_B$) | | | |
| [wt%] | $N_2$ | $O_2$ | $CO_2$ | $CH_4$ | $H_2$ | He | $CO_2/N_2$ | $CO_2/CH_4$ | $H_2/CH_4$ | $H_2/N_2$ | $O_2/N_2$ |
| 0 | 56 | 199 | 43 | 15 | 4459 | 5780 | 0.77 | 2.86 | 299 | 80 | 3.59 |
| 10 | 66 | 305 | 66 | 22 | 6804 | 8783 | 1.00 | 3.02 | 313 | 104 | 4.66 |
| 25 | 46 | 194 | 48 | 13 | 5234 | 4341 | 1.06 | 3.67 | 398 | 115 | 4.26 |
| **MIL-177(Ti)** | | | Sx [$cm^3$(STP) $cm^{-3}$ $bar^{-1}$] | | | | | α ($S_A/S_B$) | | | |
| [wt%] | $N_2$ | $O_2$ | $CO_2$ | $CH_4$ | $H_2$ | He | $CO_2/N_2$ | $CO_2/CH_4$ | $H_2/CH_4$ | $H_2/N_2$ | $O_2/N_2$ |
| 0 | 6.14 | 6.69 | 109 | 37.0 | 1.05 | 0.28 | 17.8 | 2.93 | 0.03 | 0.17 | 1.10 |
| 10 | 4.95 | 7.10 | 70.4 | 21.6 | 1.00 | 0.27 | 14.2 | 3.26 | 0.05 | 0.20 | 1.43 |
| 25 | 5.36 | 3.57 | 84.21 | 28.61 | 0.73 | 0.22 | 15.7 | 2.94 | 0.03 | 0.14 | 0.67 |
| **PIM-EA-TB/ MIL-177(Ti)_T°C** | | | | | | | | | | | |
| **MIL-177(Ti)** | | | Permeability [Barrer] | | | | | α ($P_A/P_B$) | | | |
| [wt%] | $N_2$ | $O_2$ | $CO_2$ | $CH_4$ | $H_2$ | He | $CO_2/N_2$ | $CO_2/CH_4$ | $H_2/CH_4$ | $H_2/N_2$ | $O_2/N_2$ |
| 0 | 375 | 1636 | 5125 | 622 | 5500 | 1940 | 13.7 | 8.24 | 8.84 | 14.7 | 4.36 |
| 10 | 252 | 1188 | 3803 | 349 | 5184 | 1948 | 15.1 | 10.9 | 14.9 | 20.6 | 4.71 |
| 25 | 255 | 1098 | 3681 | 370 | 4450 | 1765 | 14.4 | 10.0 | 12.0 | 17.4 | 4.30 |
| **MIL-177(Ti)** | | | Dx [10-12 $m^2s^{-1}$] | | | | | α ($D_A/D_B$) | | | |
| [wt%] | $N_2$ | $O_2$ | $CO_2$ | $CH_4$ | $H_2$ | He | $CO_2/N_2$ | $CO_2/CH_4$ | $H_2/CH_4$ | $H_2/N_2$ | $O_2/N_2$ |
| 0 | 36 | 160 | 36 | 14 | 4260 | 4899 | 1.00 | 2.54 | 298 | 118 | 4.43 |
| 10 | 25 | 128 | 30 | 8 | 3270 | 4678 | 1.22 | 3.95 | 426 | 131 | 5.12 |
| 25 | 38 | 156 | 45 | 13 | 3681 | 3921 | 1.19 | 3.53 | 290 | 98 | 4.14 |
| **MIL-177(Ti)** | | | Sx [$cm^3$(STP) $cm^{-3}$ $bar^{-1}$] | | | | | α ($S_A/S_B$) | | | |
| [wt%] | $N_2$ | $O_2$ | $CO_2$ | $CH_4$ | $H_2$ | He | $CO_2/N_2$ | $CO_2/CH_4$ | $H_2/CH_4$ | $H_2/N_2$ | $O_2/N_2$ |
| 0 | 7.79 | 7.67 | 106 | 32.6 | 0.97 | 0.30 | 13.6 | 3.24 | 0.03 | 0.12 | 0.98 |
| 10 | 6.01 | 5.65 | 84.6 | 27.2 | 0.94 | 0.22 | 14.1 | 3.11 | 0.03 | 0.16 | 0.94 |
| 25 | 5.04 | 5.28 | 61.3 | 21.3 | 0.91 | 0.34 | 12.1 | 2.88 | 0.04 | 0.18 | 1.05 |
| **PIM-EA-TB/ MIL-177(Ti)_Aged** | | | | | | | | | | | |
| **MIL-177(Ti)** | | | Permeability [Barrer] | | | | | α ($P_A/P_B$) | | | |

| [wt%] | $N_2$ | $O_2$ | $CO_2$ | $CH_4$ | $H_2$ | He | $CO_2/N_2$ | $CO_2/CH_4$ | $H_2/CH_4$ | $H_2/N_2$ | $O_2/N_2$ |
|---|---|---|---|---|---|---|---|---|---|---|---|
| 0 (800d) | 94 | 375 | 1511 | 139 | 1225 | 478 | 16.1 | 10.91 | 8.84 | 13.0 | 3.98 |
| 25 (30d) | 150 | 729 | 2347 | 181 | 3750 | 1473 | 15.6 | 13.0 | 20.8 | 24.9 | 4.85 |
| **MIL-177(Ti)** | | | Dx [10-12 $m^2s^{-1}$] | | | | | | α ($D_A/D_B$) | | |
| [wt%] | $N_2$ | $O_2$ | $CO_2$ | $CH_4$ | $H_2$ | He | $CO_2/N_2$ | $CO_2/CH_4$ | $H_2/CH_4$ | $H_2/N_2$ | $O_2/N_2$ |
| 0 | 20 | 73 | 21 | 6 | 1885 | 2777 | 1.06 | 3.34 | 299 | 94.5 | 3.67 |
| 20 | 30 | 130 | 35 | 9 | 3815 | 6405 | 1.17 | 3.89 | 423 | 127 | 4.33 |
| **MIL-177(Ti)** | | | Sx [$cm^3$(STP) $cm^{-3}$ $bar^{-1}$] | | | | | | α ($S_A/S_B$) | | |
| [wt%] | $N_2$ | $O_2$ | $CO_2$ | $CH_4$ | $H_2$ | He | $CO_2/N_2$ | $CO_2/CH_4$ | $H_2/CH_4$ | $H_2/N_2$ | $O_2/N_2$ |
| 0 | 3.53 | 3.85 | 53.9 | 17.3 | 0.49 | 0.13 | 15.2 | 3.27 | 0.03 | 0.14 | 1.08 |
| 25 | 3.76 | 4.21 | 50.3 | 15.0 | 0.74 | 0.17 | 13.4 | 3.34 | 0.05 | 0.20 | 1.12 |

**Table S-3** Pure gas permeability, solubility and diffusion coefficients, and respective selectivity of neat PIM-TMN-Trip and PIM-TMN-Trip/MIL-101 MMMs for MeOH, thermal and aging conditioning of membranes

| **PIM-TMN-Trip/ MIL-101(Cr)_MeOH** | | | | | | | | | | | |
|---|---|---|---|---|---|---|---|---|---|---|---|
| **MIL-101(Cr)** | Permeability [Barrer] | | | | | | α ($P_A/P_B$) | | | | |
| [wt%] | $N_2$ | $O_2$ | $CO_2$ | $CH_4$ | $H_2$ | He | $CO_2/N_2$ | $CO_2/CH_4$ | $H_2/CH_4$ | $H_2/N_2$ | $O_2/N_2$ |
| 0 | 3525 | 8777 | 40728 | 6071 | 16279 | 5823 | 11.6 | 6.71 | 2.68 | 4.62 | 2.49 |
| 10 | 1656 | 7462 | 32997 | 3508 | 17141 | 6228 | 19.9 | 9.41 | 4.89 | 10.4 | 4.51 |
| **MIL-101(Cr)** | Dx [10-12 $m^2s^{-1}$] | | | | | | α ($D_A/D_B$) | | | | |
| [wt%] | $N_2$ | $O_2$ | $CO_2$ | $CH_4$ | $H_2$ | He | $CO_2/N_2$ | $CO_2/CH_4$ | $H_2/CH_4$ | $H_2/N_2$ | $O_2/N_2$ |
| 0 | 526 | 1355 | 497 | 297 | 14746 | 16900 | 0.95 | 1.67 | 49.6 | 28.0 | 2.58 |
| 10 | 397 | 1465 | 410 | 252 | 15252 | 17611 | 1.03 | 1.63 | 50.5 | 38.4 | 3.70 |
| **MIL-101(Cr)** | Sx [$cm^3$(STP) $cm^{-3}$ $bar^{-1}$] | | | | | | α ($S_A/S_B$) | | | | |
| [wt%] | $N_2$ | $O_2$ | $CO_2$ | $CH_4$ | $H_2$ | He | $CO_2/N_2$ | $CO_2/CH_4$ | $H_2/CH_4$ | $H_2/N_2$ | $O_2/N_2$ |
| 0 | 5.03 | 4.86 | 61,4 | 15,3 | 0,83 | 0.26 | 12.2 | 4.01 | 0.05 | 0.16 | 0.97 |
| 10 | 3.13 | 3.82 | 60.4 | 10.4 | 0.84 | 0.26 | 19.3 | 5.78 | 0.08 | 0.27 | 1.22 |
| **PIM-TMN-Trip/ MIL-101(Cr)_T°C** | | | | | | | | | | | |
| **MIL-101(Cr)** | Permeability [Barrer] | | | | | | α ($P_A/P_B$) | | | | |
| [wt%] | $N_2$ | $O_2$ | $CO_2$ | $CH_4$ | $H_2$ | He | $CO_2/N_2$ | $CO_2/CH_4$ | $H_2/CH_4$ | $H_2/N_2$ | $O_2/N_2$ |
| 0 | 1833 | 5950 | 26983 | 2591 | 13413 | 4876 | 14.7 | 10.4 | 5.18 | 7.32 | 3.25 |
| 10 | 2047 | 6156 | 27001 | 3609 | 13249 | 5194 | 13.2 | 7.48 | 3.67 | 6.47 | 3.01 |
| **MIL-101(Cr)** | Dx [10-12 m2s-1] | | | | | | α ($D_A/D_B$) | | | | |
| [wt%] | $N_2$ | $O_2$ | $CO_2$ | $CH_4$ | $H_2$ | He | $CO_2/N_2$ | $CO_2/CH_4$ | $H_2/CH_4$ | $H_2/N_2$ | $O_2/N_2$ |
| 0 | 278 | 882 | 357 | 114 | 11517 | 12299 | 1.28 | 3.13 | 101 | 41.4 | 3.17 |
| 10 | 590 | 1267 | 477 | 329 | 12962 | 13256 | 0.81 | 1.45 | 39.4 | 22.0 | 2.15 |
| **MIL-101(Cr)** | Sx [$cm^3$(STP) $cm^{-3}$ $bar^{-1}$] | | | | | | α ($S_A/S_B$) | | | | |
| [wt%] | $N_2$ | $O_2$ | $CO_2$ | $CH_4$ | $H_2$ | He | $CO_2/N_2$ | $CO_2/CH_4$ | $H_2/CH_4$ | $H_2/N_2$ | $O_2/N_2$ |
| 0 | 4.94 | 5.06 | 56.7 | 17.1 | 0.87 | 0.30 | 11.5 | 3.32 | 0.05 | 0.18 | 1.03 |
| 10 | 2.60 | 3.64 | 42.4 | 8.24 | 0.77 | 0.29 | 16.3 | 5.15 | 0.09 | 0.29 | 1.40 |
| **PIM-TMN-Trip/ MIL-101(Cr)_Aged** | | | | | | | | | | | |
| **MIL-101(Cr)** | Permeability [Barrer] | | | | | | α ($P_A/P_B$) | | | | |
| [wt%] | $N_2$ | $O_2$ | $CO_2$ | $CH_4$ | $H_2$ | He | $CO_2/N_2$ | $CO_2/CH_4$ | $H_2/CH_4$ | $H_2/N_2$ | $O_2/N_2$ |
| 0 (700d) | 680 | 2774 | 11856 | 877 | 9353 | 3788 | 17.43 | 13.53 | 10.67 | 13.75 | 4.08 |
| 10 (700d) | 690 | 2658 | 11529 | 927 | 8543 | 3596 | 16.70 | 12.44 | 9.22 | 12.37 | 3.85 |
| (2000d) | 665 | 2531 | 10528 | 895 | 8207 | 3453 | 15.84 | 11.76 | 12.3 | 12.3 | 3.81 |

**Table S-4** Pure gas permeability, solubility and diffusion coefficients, and respective selectivity of neat PIM-TMN-Trip and PIM-TMN-Trip/MIL-177(Ti) MMMs for MeOH, thermal and aging conditioning of membranes

| **PIM-TMN-Trip/ MIL-177(Ti)_MeOH** | | | | | | | | | | | |
|---|---|---|---|---|---|---|---|---|---|---|---|
| **MIL-177(Ti)** | Permeability [Barrer] | | | | | | α ($P_A/P_B$) | | | | |
| [wt%] | $N_2$ | $O_2$ | $CO_2$ | $CH_4$ | $H_2$ | He | $CO_2/N_2$ | $CO_2/CH_4$ | $H_2/CH_4$ | $H_2/N_2$ | $O_2/N_2$ |
| 0 | 3525 | 8777 | 40728 | 6071 | 16279 | 5823 | 11.6 | 6.71 | 2.68 | 4.62 | 2.49 |
| 10 | 1253 | 5692 | 22777 | 2405 | 17084 | 6969 | 18.2 | 9.47 | 7.10 | 13.6 | 4.54 |
| **MIL-177(Ti)** | Dx [10-12 $m^2s^{-1}$] | | | | | | α ($D_A/D_B$) | | | | |
| [wt%] | $N_2$ | $O_2$ | $CO_2$ | $CH_4$ | $H_2$ | He | $CO_2/N_2$ | $CO_2/CH_4$ | $H_2/CH_4$ | $H_2/N_2$ | $O_2/N_2$ |
| 0 | 526 | 1355 | 497 | 297 | 14746 | 16900 | 0.95 | 1.67 | 49.6 | 28.0 | 2.58 |
| 10 | 737 | 1464 | 498 | 326 | 15253 | 17516 | 0.68 | 1.53 | 46.8 | 20.7 | 1.99 |
| **MIL-177(Ti)** | Sx [$cm^3$(STP) $cm^{-3}$ $bar^{-1}$] | | | | | | α ($S_A/S_B$) | | | | |
| [wt%] | $N_2$ | $O_2$ | $CO_2$ | $CH_4$ | $H_2$ | He | $CO_2/N_2$ | $CO_2/CH_4$ | $H_2/CH_4$ | $H_2/N_2$ | $O_2/N_2$ |
| 0 | 5.03 | 4.86 | 61.45 | 15.32 | 0.83 | 0.26 | 12.2 | 4.01 | 0.05 | 0.16 | 0.97 |
| 10 | 1.27 | 2.92 | 34.29 | 5.54 | 0.84 | 0.32 | 26.9 | 6.20 | 0.15 | 0.66 | 2.29 |
| **PIM-TMN-Trip/MIL-177 (Ti)_T°C** | | | | | | | | | | | |
| **MIL-177(Ti)** | Permeability [Barrer] | | | | | | α ($P_A/P_B$) | | | | |
| [wt%] | $N_2$ | $O_2$ | $CO_2$ | $CH_4$ | $H_2$ | He | $CO_2/N_2$ | $CO_2/CH_4$ | $H_2/CH_4$ | $H_2/N_2$ | $O_2/N_2$ |
| 0 | 1833 | 5950 | 26983 | 2591 | 13413 | 4876 | 14.7 | 10.4 | 5.2 | 7.32 | 3.2 |
| 10 | 1309 | - | 20745 | 2236 | 12322 | 5152 | 15.9 | 9.28 | 5.51 | 9.41 | - |
| **MIL-177(Ti)** | Dx [10-12 m2s-1] | | | | | | α ($D_A/D_B$) | | | | |
| [wt%] | $N_2$ | $O_2$ | $CO_2$ | $CH_4$ | $H_2$ | He | $CO_2/N_2$ | $CO_2/CH_4$ | $H_2/CH_4$ | $H_2/N_2$ | $O_2/N_2$ |
| 0 | 278 | 882 | 357 | 114 | 11517 | 12299 | 1.28 | 3.13 | 101 | 41.4 | 3.17 |
| 10 | 662 | - | 481 | 461 | 11929 | 13139 | 0.73 | 1.04 | 25.9 | 18.0 | - |
| **MIL-177(Ti)** | Sx [$cm^3$(STP) $cm^{-3}$ $bar^{-1}$] | | | | | | α ($S_A/S_B$) | | | | |
| [wt%] | $N_2$ | $O_2$ | $CO_2$ | $CH_4$ | $H_2$ | He | $CO_2/N_2$ | $CO_2/CH_4$ | $H_2/CH_4$ | $H_2/N_2$ | $O_2/N_2$ |
| 0 | 4.94 | 5.06 | 56.7 | 17.0 | 0.87 | 0.30 | 11.5 | 3.33 | 0.05 | 0.18 | 1.03 |
| 10 | 1.48 | - | 32.3 | 3.64 | 0.77 | 0.29 | 21.8 | 8.89 | 0.21 | 0.52 | - |
| **PIM-TMN-Trip/MIL-177(Ti)_Aged** | | | | | | | | | | | |
| **MIL-177(Ti)** | Permeability [Barrer] | | | | | | α ($P_A/P_B$) | | | | |
| [wt%] | $N_2$ | $O_2$ | $CO_2$ | $CH_4$ | $H_2$ | He | $CO_2/N_2$ | $CO_2/CH_4$ | $H_2/CH_4$ | $H_2/N_2$ | $O_2/N_2$ |
| 0 (700d) | 680 | 2774 | 11856 | 877 | 9353 | 3788 | 17.43 | 13.53 | 10.67 | 13.75 | 4.08 |
| 10 (700d) | 524 | 2169 | 9126 | 721 | 8373 | 3823 | 17.41 | 12.66 | 11.61 | 15.98 | 4.14 |

**Table S-5** $CO_2$ permeability over an aging time of an almost 2 years for neat polymers and their respective MMMs.

| | PIM-TMN-Trip | | 10%MIL-101(Cr) | | 10%MIL-177(Ti) |
|---|---|---|---|---|---|
| Aging days | $PCO_2$ | Aging days | $PCO_2$ | Aging days | $PCO_2$ |
| 1 | 40728 | 1 | 32997 | 1 | 22777 |
| 2 | 26983 | 2 | 27001 | 36 | 11278 |
| 365 | 14054 | 464 | 14610 | 200 | 11250 |
| 700 | 11856 | 700 | 11529 | 365 | 11278 |
| - | - | 2000 | 10528 | 703 | 9126 |
| | PIM-EA-TB | | 20%MIL-101(Cr) | | 10%MIL-177(Ti) |
| Aging days | $PCO_2$ | Aging days | $PCO_2$ | Aging days | $PCO_2$ |
| 1 | 6231 | 1 | 10313 | 1 | 6198 |
| 2 | 5125 | 2 | 9238 | 2 | 3803 |
| 100 | 2644 | 30 | 5891 | 30 | 2347 |
| 860 | 1512 | 1500 | 3379 | - | - |
| - | - | 2000 | 3463 | 2000 | 816 |

**Table S-6** Mixed gas permeability and selectivity for the PIM-TMN-Trip/MIL-101(Cr) and PIM-EA-TB MMMs in binary mixtures $CO_2/CH_4$ (35:65 Vol%), $CO_2/N_2$ (15:85 Vol%) and $O_2/N_2$ (20:80 Vol%)

| **PIM-TMN-Trip/ MIL-101(Cr)_aged 20159 days** | | | |
|---|---|---|---|
| Mixture $CO_2/CH_4$ (35:65 Vol%) | | | |
| Permeability [Barrer] | | | $\alpha$ ($P_A/P_B$) |
| Pressure [bar] | $CO_2$ | $CH_4$ | $CO_2/CH_4$ |
| 1 | 15671 | 932 | 16.8 |
| 2 | 13638 | 929 | 14.7 |
| 3 | 12702 | 946 | 13.4 |
| 4 | 12037 | 966 | 12.5 |
| 5 | 11503 | 986 | 11.7 |
| 6 | 11104 | 995 | 11.2 |
| 5.5 | 11431 | 1010 | 11.3 |
| 4.5 | 12036 | 1036 | 11.6 |
| 3.5 | 12770 | 1033 | 12.4 |
| 2.5 | 13621 | 1039 | 13.1 |
| 1.5 | 14743 | 1028 | 14.3 |
| 1 | 15481 | 1015 | 15.2 |
| Mixture $CO_2/N_2$ (15:85 Vol%) | | | |
| Permeability [Barrer] | | | $\alpha$ ($P_A/P_B$) |

| Pressure [bar] | $CO_2$ | $N_2$ | $CO_2/N_2$ |
|---|---|---|---|
| 1 | 15529 | 710 | 21.9 |
| 2 | 14088 | 705 | 20.0 |
| 3 | 13150 | 698 | 18.8 |
| 4 | 12449 | 694 | 17.9 |
| 5 | 11923 | 693 | 17.2 |
| 6 | 11470 | 689 | 16.6 |
| 5.5 | 11698 | 694 | 16.9 |
| 4.5 | 12219 | 703 | 17.4 |
| 3.5 | 12881 | 709 | 18.2 |
| 2.5 | 13701 | 715 | 19.2 |
| 1.5 | 14792 | 717 | 20.6 |
| 1 | 15646 | 720 | 21.7 |

| Mixture $O_2/N_2$ (15:85 Vol%) | | | |
|---|---|---|---|
| Permeability [Barrer] | | | $\alpha$ ($P_A/P_B$) |
| Pressure [bar] | $O_2$ | $N_2$ | $O_2/N_2$ |
| 1 | 2559 | 522 | 4.90 |
| 2 | 2597 | 516 | 5.03 |
| 3 | 2624 | 518 | 5.07 |
| 4 | 2643 | 521 | 5.07 |
| 5 | 2658 | 526 | 5.05 |
| 6 | 2671 | 528 | 5.06 |
| 5.5 | 2717 | 533 | 5.10 |
| 4.5 | 2778 | 539 | 5.16 |
| 3.5 | 2843 | 540 | 5.27 |
| 2.5 | 2898 | 542 | 5.35 |
| 1.5 | 2936 | 535 | 5.49 |
| 1 | 2973 | 529 | 5.62 |

| **PIM-EA-TB/MIL-101(Cr)_MeOH** | | | |
|---|---|---|---|
| Mixture $CO_2/CH_4$ (35:65 Vol%) | | | |
| Permeability [Barrer] | | | $\alpha$ ($P_A/P_B$) |
| Pressure [bar] | $CO_2$ | $CH_4$ | $CO_2/CH_4$ |
| 1 | 2146 | 86 | 16.8 |
| 2 | 2079 | 93 | 14.7 |
| 3 | 2149 | 95 | 13.4 |
| 4 | 2146 | 99 | 12.5 |
| 5 | 2132 | 102 | 11.7 |
| 6 | 2126 | 105 | 11.2 |
| 5.5 | 2132 | 104 | 11.3 |

| | | | |
|---|---|---|---|
| 4.5 | 2158 | 102 | 11.6 |
| 3.5 | 2180 | 101 | 12.4 |
| 2.5 | 2197 | 100 | 13.1 |
| 1.5 | 2118 | 103 | 14.3 |
| 1 | 2103 | 105 | 15.2 |

| Mixture $CO_2/N_2$ (15:85 Vol%) | | | |
|---|---|---|---|
| Permeability [Barrer] | | | $\alpha$ ($P_A/P_B$) |
| Pressure [bar] | $CO_2$ | $N_2$ | $CO_2/N_2$ |
| 1 | 2372 | 105 | 22.6 |
| 2 | 2425 | 96 | 25.3 |
| 3 | 2408 | 90 | 26.8 |
| 4 | 2357 | 87 | 27.2 |
| 5 | 2372 | 84 | 28.1 |
| 6 | 2330 | 82 | 28.4 |
| 5.5 | 2355 | 82 | 28.6 |
| 4.5 | 2384 | 84 | 28.3 |
| 3.5 | 2328 | 86 | 27.2 |
| 2.5 | 2353 | 88 | 26.8 |
| 1.5 | 2364 | 94 | 25.3 |
| 1 | 2343 | 91 | 25.6 |
| Mixture $O_2/N_2$ (15:85 Vol%) | | | |
| Permeability [Barrer] | | | $\alpha$ ($P_A/P_B$) |
| Pressure [bar] | $O_2$ | $N_2$ | $O_2/N_2$ |
| 1 | 470 | 99 | 4.74 |
| 2 | 470 | 86 | 5.46 |
| 3 | 472 | 87 | 5.40 |
| 4 | 473 | 88 | 5.34 |
| 5 | 475 | 87 | 5.49 |
| 6 | 476 | 88 | 5.41 |
| 5.5 | 481 | 90 | 5.33 |
| 4.5 | 489 | 93 | 5.24 |
| 3.5 | 493 | 99 | 5.00 |
| 2.5 | 496 | 105 | 4.74 |
| 1.5 | 493 | 113 | 4.38 |
| 1 | 494 | 123 | 4.00 |